



TECHNISCHE
UNIVERSITÄT
WIEN
Vienna | Austria

DIPLOMARBEIT

Geometry and Interactive Design of Curved Creases

Ausgeführt am Institut für
Diskrete Mathematik und Geometrie
der Technischen Universität Wien

unter der Anleitung von
O. Univ. Prof. Dr. Helmut Pottmann

durch
Klara Mundilova, BSc

Datum

Unterschrift

Abstract

This thesis discusses curved creases from a theoretic and an applied point of view:

On the one hand, we utilize differential geometry to describe curved creases between developable surfaces by five quantities. We conclude that defining three of them appropriately determines the remaining two except in some special cases. Apart from degenerated folds, we also address two special types of folds: the planar crease, i.e. the rulings of the corresponding developable surfaces are reflected on a plane, and creases of constant angle. The latter crease curves are known as pseudo-geodesics in classical differential geometry. By combining these classical results with our approaches, we examine pseudo-geodesics on cylinders and cones. Furthermore, a connection between bi-cylindrical, bi-conical and cylindro-conical creases of constant angle and geodesics on quadrics can be established.

The applied approach is based on the work made by Tang et al. on the interactive design of curved creases. We utilize their proposed guided projection algorithm to solve an optimization problem for B-spline representations of developable surfaces with creases, and discuss the needed variables and constraints. Finally, we present some examples obtained from the author's implementation.

Contents

0	Introduction	1
0.1	Related Work	3
0.2	Overview	4
0.3	Acknowledgements	5
I	Differential Geometry of Curved Creases	7
1	Analytic description of curved creases	9
2	Degenerate and planar folds	18
2.1	Complete folds	18
2.2	Trivial folds	18
2.3	Planar folds	19
3	Curved creases of constant angle	21
3.1	Curved creases of constant angle on cylinders	22
3.1.1	Geometric approach	22
3.1.2	Analytic approach	22
3.1.3	Curved creases of constant angle on cylinders of revolution	24
3.2	Curved creases of constant angle on cones	24
3.2.1	Geometric approach	24
3.2.2	Analytic approach	26
3.2.3	Curved creases of constant angle on cones of revolution	27
3.3	Curved creases of constant angle between cylinders and cones	31
3.3.1	Geometric description	31

3.3.2	Other interpretations	35
3.3.3	Analytic description	38
II	Optimization	45
4	Algorithmic setup	47
4.1	Algorithm	47
4.2	Weighted linear least squares	48
4.3	Interactive design	48
5	Computational setup	49
5.1	Theoretical background	49
5.2	Detailed discussion of variables and constraints	50
5.2.1	Developability constraint	51
5.2.2	Normals as variables	51
5.2.3	Unit-length constraint for normals	54
5.2.4	Curved crease condition	54
5.2.5	Isometry constraints	56
5.2.6	Fairness energy constraint	57
5.2.7	Regularization constraint	58
5.3	Combinatorial consistency	59
5.4	Accompanying program	60
5.5	Further implementation features	60
5.6	Parameters	61
5.6.1	Robustness	63
5.6.2	Detailed discussion of a good result	66
5.7	Convergence	68
6	Further examples	71
6.1	Moebius strip	71
6.2	Composite developable	72
	Bibliography	76

Chapter 0

Introduction

This thesis investigates the geometry of the behaviour of planar sheets when folded along curves without stretching or tearing, i.e. developable surface patches joined at curved creases.

Developable surfaces, often also referred to as single curved surfaces, have various applications, particularly in architecture, the manufacturing industry, e.g. the construction of ship hulls, in art and design. The materials used for the production of those objects are glass, metal, paper and wood.

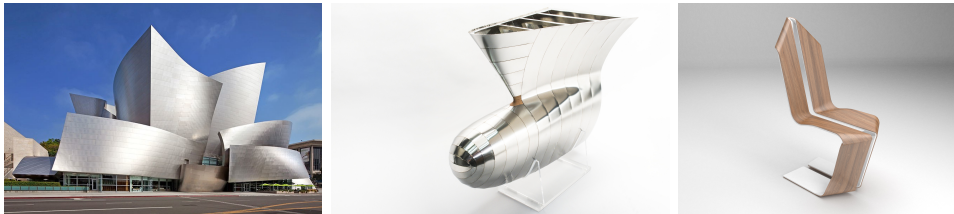


Figure 1: Frank Gehry's *Walt Disney Concert Hall* in Los Angeles (left), ship hull made of metal panels by EvoluteTools DLoft (middle) and *A4 Chair* by Chris Kim (right)

As smooth developable surfaces are just combinations of parts of cones, cylinders and tangent surfaces, the resulting shapes are limited. Permitting also folding of the processed material in the design process, i.e. the generalization to developables with creases, yields a broader variety of possible composite surfaces, in case of paper also referred to as curved origami. The full extent of the possible shapes has not been exhausted yet.



Figure 2: curved origami: Ron Resch's *Kissing Cones* (left) and Richard Sweeney's *Embrace* (right)

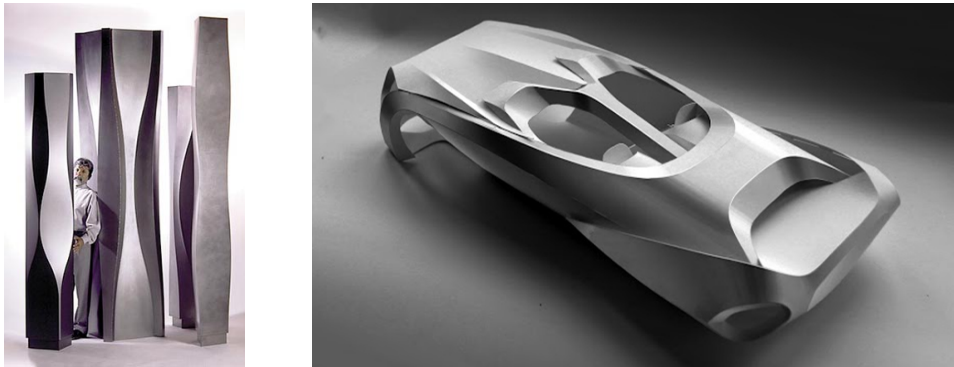


Figure 3: curved creases manufactured through bending sheets of metal: Haresh Lalvani with his metal columns (left) and Gregory Epps' *Bentley and Kyungeun KO* (right)

Curved creases are also used for production purposes, e.g. when it comes to packing objects such as candy. There, a surface, also called a shoulder, leads the packing material, usually paper or plastic, from a horizontal roll to a vertical cylinder. After sealing the material on the vertical side and on the bottom, the resulting cylinder can be filled with content. Pulling the bag downward, sealing it at the top and cutting it off yields the starting configuration and the process can repeat itself. For high speed packaging, the material should be guided without disturbances, i.e. without tearing or stretching. Not surprisingly, the shoulder is therefore often chosen to be a curved crease.

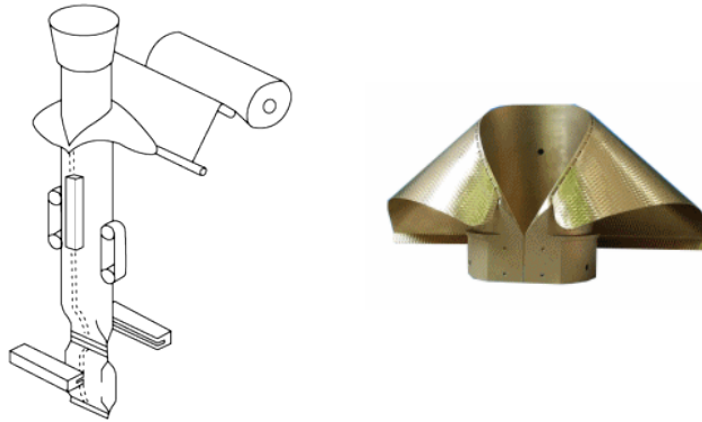


Figure 4: schematic drawing of a packaging machine¹ and a round shoulder manufactured by TOSS

0.1 Related Work

Due to the various applications mentioned above, there are different approaches to treating curved folds. An overview is given in [5].

The first fundamental mathematical treatment was done by Huffman in [8]. Apart from his theoretic results, he is also known for his designs, e.g. the *Hexagonal Column*, see Fig. 5. An insight to his work is given in [4] and [10].

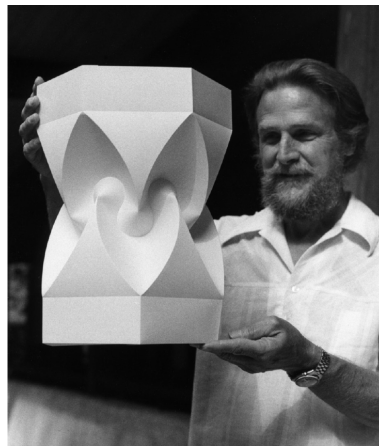


Figure 5: Richard Huffman with his *Hexagonal Column*

¹from <http://unionkehlibar.com/imgs/vffs-forming-tube.gif>, 8.5.2017

Further differential geometric approaches were published by Fuchs and Tabaschnikov in [7] and new characterizations and special cases are discussed by Demaine et al. in [2] and [3]. Moreover, theoretic results on shoulders for packaging machines were obtained by Boersma and Molenaar in [1]. Furthermore, Röschel investigates curved creases of constant angle between cylinders in [16]. As curved creases of constant angles are special cases of pseudo-geodesics of two surfaces, some information is contained in Wunderlich’s results from 1950 in [19], [20], [21] and [22] as special cases.

The differential geometric theory gives a deeper understanding of the resulting shapes. For example, folds obtained by reflection on a plane are discussed in [14]. Another prominent example, the folding of an annular circular strip along a central circular curve, is described by Dias et al. in [6]. Nevertheless, the surfaces and creases encountered in practice are in general not convenient for mathematical treatment. Therefore, the flexibility of approximating approaches is better suited for applications.

Kilian et al. discuss curved creases from a discrete differential perspective in [9]. They introduce an optimization algorithm, which allows to compute discrete developables with curved folds that are isometric to a given planar sheet. In [17], Tachi and Epps present their tool to fold discrete approximations for prescribed rulings.

Finally, a smooth approximation with B-splines for the interactive design of curved creases is proposed by Tang et al. in [18]. The second part of this thesis is based on their approach through powerful optimization.

0.2 Overview

This work is organized in two parts. The first three chapters investigate the differential geometry. The second part consists of the remaining chapters and is dedicated to the algorithmic treatment of curved creases.

In the first chapter, we introduce the necessary notation and investigate formulations of the developable and curved crease conditions. In particular, we collect five quantities defining a crease and conclude, that choosing three of them appropriately yields the other two. Then, the second chapter discusses two special cases of curved creases, namely degenerated and planar folds. The remaining special case of creases of constant angle is investigated in the third chapter. Based on Wunderlich’s results, we are able to describe creases of constant angle, where one of the surfaces is either a cylinder or a cone. We obtain explicit parametrizations for the corresponding rotational surfaces. The resulting curves can be compared with catenaries. Furthermore, we establish a connection between geodesics on rotational quadrics

and bi-cylindrical, bi-conical and cylindro-conical creases of constant angle. The second part starts in chapter four with the description of the guided projection algorithm used for the optimization in the implementation of a Rhinoceros3D plug-in for the interactive design of developable surfaces. The variables and constraints used in this optimization setup are discussed in chapter five. Finally, we present some examples of optimized developables with curved creases in the last chapter.

0.3 Acknowledgements

First, I would like to thank Professor Helmut Pottmann for his supervision and instructive suggestions, and Dr. Simon Flöry, who gave me the opportunity to implement the presented plug-in during my employment at his company Rechenraum, and supported me with his valuable insights in optimization.

Furthermore, I am grateful for the valuable discussions with colleagues and friends, especially Dr. Martin Peternell, Andreas Fuchs and Alexander Palmrich.

Part I

Differential Geometry of
Curved Creases

Chapter 1

Analytic description of curved creases

We want to study the geometrical behaviour of a surface, that can be obtained by folding a sheet of paper along a curve without stretching or tearing the paper. Therefore, we consider only surfaces that are composed of two developable surface patches, which, unrolled into the plane, have the same curvature along the developed crease curve.

In the following geometric approach, we will refer to a *curved crease*, to avoid lengthy formulations, as a pair of (globally defined) developable surfaces σ_1 and σ_2 , which intersect under certain conditions. Cutting these surfaces along the intersecting curve c yields four surface patches $\sigma_1^+, \sigma_1^-, \sigma_2^+$ and σ_2^- . The resulting surface pairs (σ_1^+, σ_2^-) and (σ_1^-, σ_2^+) simulate the behaviour of folding a paper along the given curve, see fig. 1.1 and fig. 1.2.

By examining three frames along the intersection curve c of these surfaces, we will introduce five quantities that describe a curved crease. Furthermore, the investigation of their interdependence obtained from the curved crease and developability conditions will yield information about the specification of a curved crease.

Let (t, n_i, b_i) denote the Darboux frames of c as curves on σ_i with the common tangent vector t . The Frenet-Serret formulas for the resp. normal curvatures κ_{n_i} , geodesic curvatures κ_{g_i} and geodesic torsions τ_i read:

$$\begin{aligned} \frac{1}{|c'|} t' &= \kappa_{n_i} n_i & -\kappa_{g_i} b_i \\ \frac{1}{|c'|} n_i' &= -\kappa_{n_i} t & \tau_i b_i \\ \frac{1}{|c'|} b_i' &= \kappa_{g_i} t & -\tau_i n_i \end{aligned}$$

If the developable surfaces σ_i are assumed to be envelopes of one-parameter families of planes spanned by t and b_i , the curvature of the curve c developed

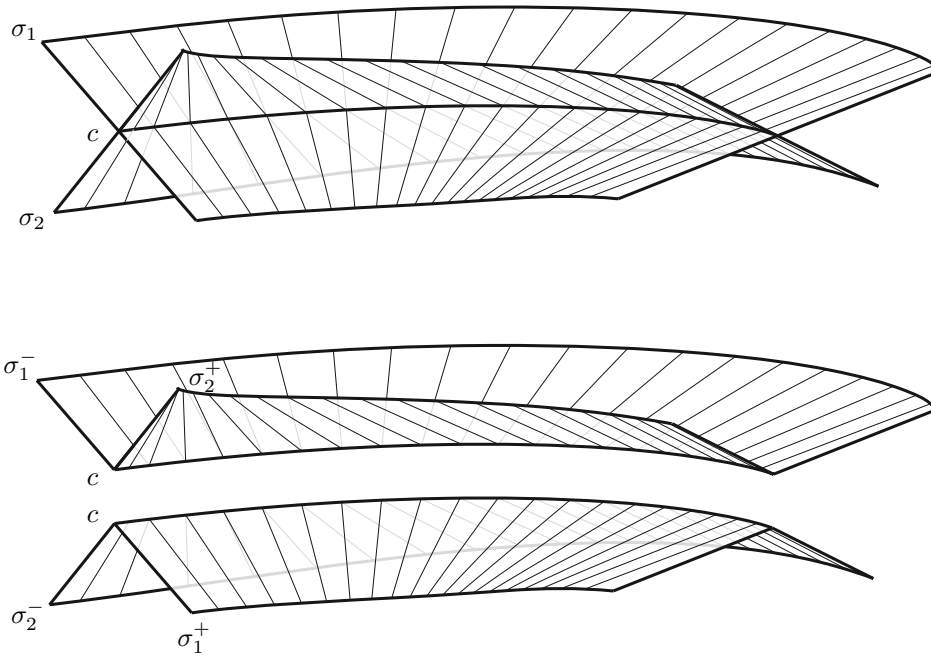


Figure 1.1: two developable surfaces σ_1 and σ_2 intersecting along a crease curve c

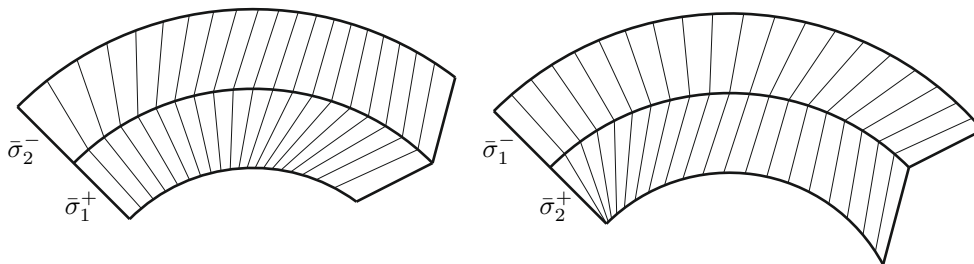


Figure 1.2: the corresponding development combinations $(\bar{\sigma}_1^+, \bar{\sigma}_2^-)$ and $(\bar{\sigma}_1^-, \bar{\sigma}_2^+)$

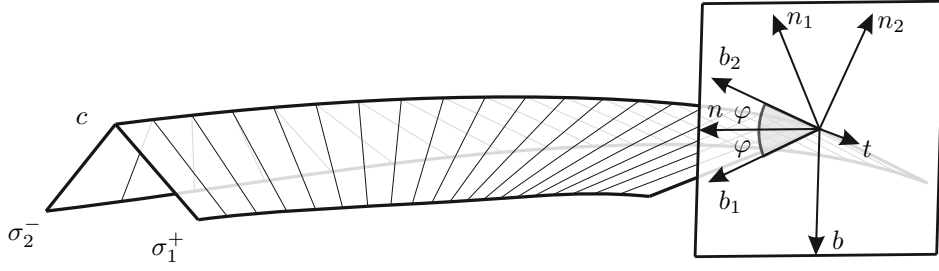


Figure 1.3: illustration of the three frames (t, n_1, b_1) , (t, n_2, b_2) and (t, n, b) of a crease curve c

w.r.t. σ_i is the corresponding geodesic curvature

$$\kappa_{g_i} = -\frac{1}{|c'|} t' b_i.$$

Since we, at least locally, demand two “components” of the developed surfaces, we exclude striction curves of σ_1 and σ_2 from our considerations. As the curves developed w.r.t. the two surfaces must coincide, the *curved crease condition* for not singular curves reads $\kappa_{g_1} = \kappa_{g_2}$ and we denote

$$\kappa_d := \kappa_{g_1} = \kappa_{g_2}.$$

The subscript d should reflect that κ_d is the curvature of the developed crease curve \bar{c} w.r.t. either one of the surfaces σ_i .

In order to unite the terms of the two frames, we will also consider the Frenet-frame of c , whose equations for the curvature κ and torsion τ read:

$$\begin{aligned} \frac{1}{|c'|} t' &= \kappa n \\ \frac{1}{|c'|} n' &= -\kappa t + \tau b \\ \frac{1}{|c'|} b' &= -\tau n \end{aligned}$$

Inserting the first relation into the curved crease condition yields $nb_1 = nb_2$. Thus the (non-trivial) curved-fold condition holds, iff the osculating plane of the curve is the bisector of the corresponding surface tangent planes. Hence, we define the enclosing angle $\varphi \in [-\pi, \pi]$ by

$$\cos \varphi = nb_1 = nb_2,$$

see fig. 1.3.

The Darboux frames can be expressed in terms of (n, b) by

$$\begin{aligned} n_1 &= -\sin \varphi n - \cos \varphi b \\ b_1 &= \cos \varphi n - \sin \varphi b \\ n_2 &= \sin \varphi n - \cos \varphi b \\ b_2 &= \cos \varphi n + \sin \varphi b \end{aligned}$$

and it can be observed that changing the sign of φ corresponds to exchanging the subscript of the frames (t, n_i, b_i) .

The curvatures and torsions in terms of the Frenet frame and the angle φ read

$$\begin{aligned}\kappa_{n_1} &= \frac{1}{|c'|} t' n_1 = -\kappa \sin \varphi \\ \kappa_{n_2} &= \frac{1}{|c'|} t' n_2 = \kappa \sin \varphi \\ \kappa_d &= -\frac{1}{|c'|} t' b_i = -\kappa \cos \varphi \\ \tau_1 &= \frac{1}{|c'|} n'_1 b_1 = \tau - \varphi' \\ \tau_2 &= \frac{1}{|c'|} n'_2 b_2 = \tau + \varphi'\end{aligned}$$

from which we conclude the relations

$$\kappa_{n_1} = -\kappa_{n_2}, \quad \tau = \frac{\tau_1 + \tau_2}{2} \quad \text{and} \quad \varphi' = \frac{\tau_2 - \tau_1}{2}.$$

Furthermore, the above equations yield

$$|\kappa_d| \leq |\kappa|,$$

which, interpreted in our setting, tell us that the crease is more strongly curved than its development.

The last describing quantities introduced are the angles $\psi_i \in [0, \pi)$ between the tangent t and the rulings r_i of the developable surface patches σ_i , defined by

$$r_i = \cos \psi_i t + \sin \psi_i b_i. \quad (1.1)$$

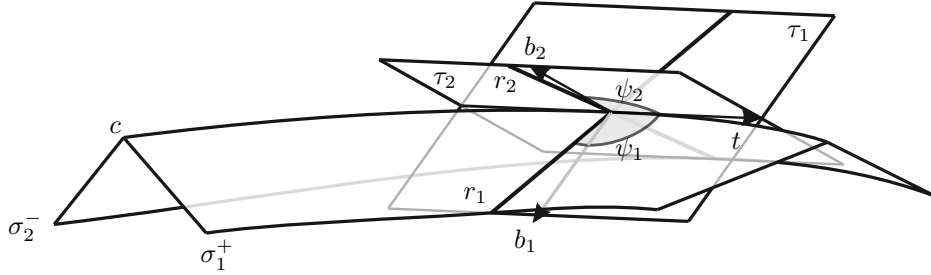


Figure 1.4: illustration of the angles ψ_1 and ψ_2

Since we forbid c to be the striction curve of σ_1 or σ_2 , $\psi_1 \neq 0$ except for isolated points.

Denoting the tangent and normal of the developed crease curve \bar{c} by \bar{t} and \bar{n} , the developed rulings \bar{r}_i read

$$\bar{r}_i = \cos \psi_i \bar{t} + \sin \psi_i \bar{n}.$$

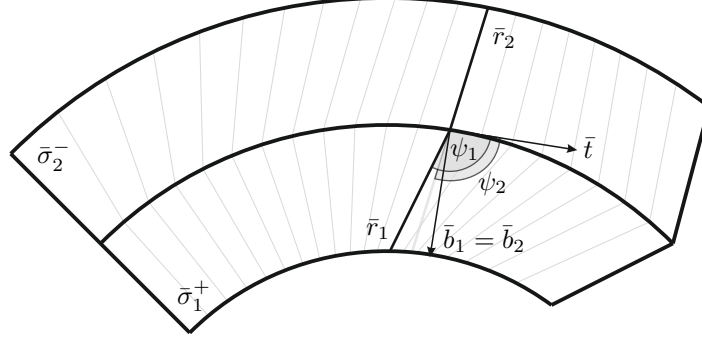


Figure 1.5: development of the surfaces in Fig. 1.4

The surface patches mentioned in the introduction can be parametrized by

$$\sigma_i^\pm(u, v) = c(u) \pm vr_i(u) \quad \text{for } v \in [0, \infty).$$

Again, changing the sign of φ results in exchanging the roles of the surface pairs (σ_1^+, σ_2^-) and (σ_1^-, σ_2^+) .

The surfaces σ_i are developable, iff r_i' lies in the tangent plane of σ_i along the ruling, that is iff $r_i' n_i = 0$. We therefore compute

$$r_i' = \sin \psi_i (\kappa_d - \psi_i') t + (\kappa_{n_i} \cos \psi_i - \tau_i \sin \psi_i) n_i + \cos \psi_i (\psi_i' - \kappa_d) b_i$$

and conclude the *developability condition*

$$\kappa_{n_i} \cos \psi_i = \tau_i \sin \psi_i. \quad (1.2)$$

The following special degenerate cases for values of φ can occur:

- *trivial fold*: iff $\varphi \equiv 0 \pmod{\pi}$, the three frames coincide and thus the surfaces do not fold.
- *complete fold*: iff $\varphi \equiv \frac{\pi}{2} \pmod{\pi}$, the directions of the rulings of the combined surface patches lie in the same plane spanned by t and b_i and the same halfspace, that is bounded by the plane orthogonal to either b_1 or b_2 .

These special cases will be discussed later in greater detail. In order to avoid them in the computations to follow, let us assume $\varphi \not\equiv 0 \pmod{\pi}$ and $\varphi \neq \pm \frac{\pi}{2}$, thus $\kappa_d \neq 0$ and $\kappa_{n_i} \neq 0$ except for isolated points whenever necessary.

Hence, equation (1.2) can be written as

$$\cot \psi_i = \frac{\tau_i}{\kappa_{n_i}}$$

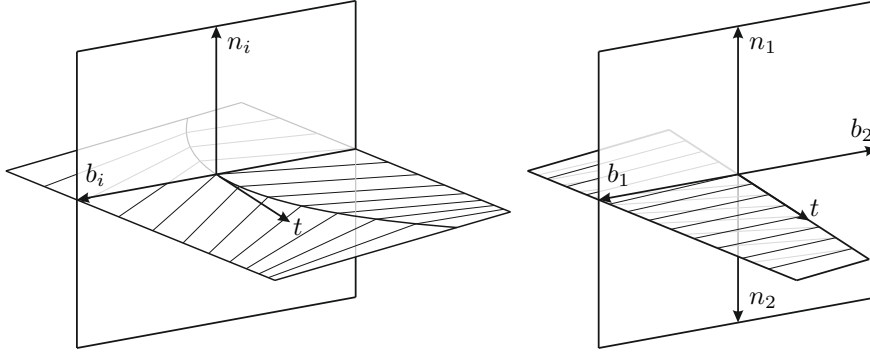


Figure 1.6: illustrations of a trivial (left) and complete fold (right)

and inserting the equations from above and utilizing $\kappa_d = -\kappa \cos \varphi$ yields

$$\cot \psi_1 = \frac{\tau - \varphi'}{\kappa_d} \cot \varphi \quad \text{and} \quad \cot \psi_2 = \frac{-\tau - \varphi'}{\kappa_d} \cot \varphi. \quad (1.3)$$

Adding and subtracting equation (1.3) for $i = 1, 2$ results in

$$\kappa_d(\cot \psi_1 + \cot \psi_2) = -2\varphi' \cot \varphi \quad (1.4)$$

and

$$\kappa_d(\cot \psi_1 - \cot \psi_2) = 2\tau \cot \varphi. \quad (1.5)$$

In particular, it can be observed that if φ is a solution of equation (1.4), $-\varphi$ is a solution as well. This corresponds to the two surface pairs obtained from a curved crease.

From the equations above, the following two special cases of a curved crease can be detected:

- *crease of constant angle:* The enclosing angle between the surfaces is constant iff $\varphi' \equiv 0$. It follows from equation (1.4) that $\cot \psi_1 \equiv -\cot \psi_2$ and thus

$$\psi_1 \equiv \pi - \psi_2,$$

that is, the developed rulings are reflected at the tangents of the developed curve.

- *planar crease:* The crease curve is planar iff τ vanishes. Equation (1.5) yields $\cot \psi_1 \equiv \cot \psi_2$ and thus

$$\psi_1 \equiv \psi_2,$$

that is, the developed directions of two corresponding rulings are collinear.

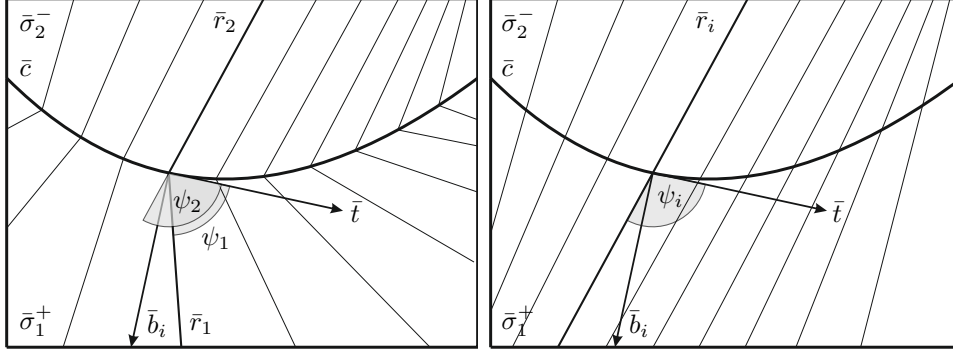


Figure 1.7: developed rulings of a crease of constant angle (left) and planar fold (right)

These cases will be discussed in greater detail in chapters 2 and 3. Let us hence for now also assume $\psi_1 \neq \psi_2$ and $\psi_1 \neq \pi - \psi_2$ except for isolated points. We will refer to non-planar folds enclosing an angle that is not constant and not $0 \pmod{\frac{\pi}{2}}$ as *generic folds*.

Eliminating κ_d from the equations (1.4) and (1.5) yields

$$\tau(\cot \psi_1 + \cot \psi_2) = \varphi'(\cot \psi_2 - \cot \psi_1). \quad (1.6)$$

We have therefore established a connection between five defining functions of a curved crease. These are:

- κ_d , the curvature of the curve developed w.r.t. the surfaces σ_i ,
- τ , the torsion of the spatial crease curve,
- φ , the angle enclosed by the osculating planes of the crease and the corresponding tangent planes of the surfaces,
- ψ_1 and ψ_2 , the angles enclosed by the tangent vector of the curve and the respective rulings of the developable surfaces σ_i .

If $\kappa_d, \tau, \varphi, \psi_1$ and ψ_2 are five sufficiently smooth function that satisfy the system of equations (1.3) - (1.5), they (locally) define a curved crease up to Euclidean displacement: the curve is determined by its curvature $\kappa = -\frac{\kappa_d}{\cos \varphi}$ and torsion τ . The two Darboux frames (t, n_i, b_i) of c are related to its Frenet frame by a normal rotation by the angle φ . Moreover, the directions of the corresponding rulings r_i are determined by ψ_i through (1.1). The resulting adjacent ruled surfaces $c(u) + vr_i$ are developable since equation (1.3) holds and enclose a curved crease due to this construction.

The following table illustrates the algebraic (a) resp. differential (d) appearances of the functions in the equations (1.3) - (1.5) and (1.6):

	κ_d	τ	φ	$\cot \psi_1$	$\cot \psi_2$
eq (1.3)	a	a	d	a	
eq (1.3)	a	a	d		a
eq (1.4)	a		d	a	a
eq (1.6)		a	d	a	a
eq (1.5)	a	a	a	a	a

Since the origin of this system of (differential) equations are the developability conditions of the surfaces, it actually consists of two independent equations from which the others were obtained: the two equations in (1.3) are equivalent to (1.4) and (1.5), since these equations result from adding and subtracting the equations in (1.3). The additional, convenient equation (1.6) holds apart of the cases of a planar fold, i.e.

$$\tau \equiv 0 \iff \cot \psi_1 \equiv \cot \psi_2 \quad (1.7)$$

and crease of constant angle, i.e.

$$\varphi' \equiv 0 \iff \cot \psi_1 \equiv -\cot \psi_2. \quad (1.8)$$

Therefore, the developability conditions from equation (1.3) are equivalent to the combination of equation (1.3) or (1.4) with (1.5). Apart from the special cases (1.7) and (1.8), this also holds for the combination of (1.6) with (1.5).

Furthermore, equations (1.3), (1.4) and (1.5) establish a relation between four of the defining functions and are linear in κ_d , τ , $\cot \psi_1$ and $\cot \psi_2$. Therefore, the specification of any three of them yields the fourth if

$$\begin{aligned} \kappa_d &\neq 0, \\ \psi_i &\neq 0 \pmod{\frac{\pi}{2}}, \\ \varphi &\neq 0 \pmod{\frac{\pi}{2}}, \end{aligned} \quad (1.9)$$

with the restriction, that in case of a planar fold or crease of constant angle, just one of the ψ_i can be defined.

Moreover, equations (1.4) and (1.5) can also be solved for φ , since equation (1.6) is separable and writing equation (1.5) in form of

$$a(t) = \varphi'(t) \cot \varphi(t) \quad \text{yields} \quad \varphi(t) = \arcsin(e^{\int a(\xi) d\xi + c}).$$

These solutions are unique for given initial values $\varphi_0 = \varphi(t_0) \in (-\pi, \pi)$.

In case of a generic fold, equation (1.5) yields a relation between all five functions κ_d , τ , φ , $\cot \psi_1$ and $\cot \psi_2$ and is also linear in all of them.

Furthermore, $\operatorname{arccot} x$ is defined for all $x \in \mathbb{R}$, $\cot \psi_i$ yields knowledge of ψ_i .

We therefore conclude:

Theorem 1.1. *Planar folds ($\tau \equiv 0$) and creases of constant angle ($\varphi = \text{const}$) are uniquely specified (up to initial values) by three of the four functions κ_d , τ , φ and ψ_1 satisfying (1.9).*

Generic folds, i.e. non-planar folds enclosing an angle that is not constant, are specified by three of the five functions κ_d , $\tau \neq 0$, $\varphi \neq \text{const}$, $\cot \psi_1$ and $\cot \psi_2 \neq \pm \cot \psi_1$ satisfying (1.9), except for the two triples $(\kappa_d, \tau, \cot \psi_i)$.

It follows, that prescribing the development, i.e. the functions $(\kappa_d, \psi_1, \psi_2)$ yields a one-parameter family of folds, where the parameter corresponds to an initial value for φ .

Another sufficient specification is obtained from the definition of the curve through κ and τ together with the angular function φ , since this information is equivalent to the triple $(\kappa_d = -\kappa \cos \varphi, \varphi, \tau)$.

Furthermore, it is also possible to construct the crease from the specification of one side, i.e. κ_d and ψ_1 , together with φ .

Chapter 2

Degenerate and planar folds

2.1 Complete folds

If $\varphi \equiv \pm\frac{\pi}{2}$, the curvature κ_d of the developed crease vanishes. That is, the only possibility for a paper to fold along a curve so that both sides overlap is just along a straight line in the development. This is supported in a more illustrative way in [7]: If γ is an arc with non-vanishing curvature and γ_+ and γ_- are two ε offsets to the concave resp. convex side, then γ_+ is strictly longer than γ , which is strictly longer than γ_- . Since folding is an isometry which preserves lengths, this is a contradiction. Not surprisingly, it follows from the equations above that $\kappa = \mp\kappa_{n_i}$, $\tau = \tau_1 = \tau_2$ and thus

$$\kappa(\cot \psi_1 - \cot \psi_2) = 0.$$

Therefore, if κ does not vanish, the developed rulings are reflected on the developed curve and thus $r_1 = -r_2$.

2.2 Trivial folds

In this case, each two associate rulings are collinear. From the formulas it follows that $\kappa_{n_1} \equiv \kappa_{n_2} \equiv 0$ and thus

$$\tau_i \sin \psi_i = \tau \sin \psi_i \equiv 0 \quad \text{for } i = 1, 2.$$

Since $\psi_i \neq 0$, the torsion vanishes. In this case of a planar crease, it seems that there is no relation between the angles ψ_1 and ψ_2 . This corresponds with the observation, that the rulings in a plane are not uniquely defined.

2.3 Planar folds

The angles of the developed rulings are equal iff the torsion vanishes, which means that the curve c is planar. The following two examples were computed as follows: Firstly, we prescribe κ_d and chose the angles ψ_i to be either (a) parallel to the y -axis or (b) orthogonal to the curve, i.e. $\psi_i \equiv \frac{\pi}{2}$.

In order to obtain the function φ , the differential equation (1.4) is solved and thus the actual folding depends on an initial value. The second example is also a crease of constant angle, since $\cot \psi_i \equiv 0$.

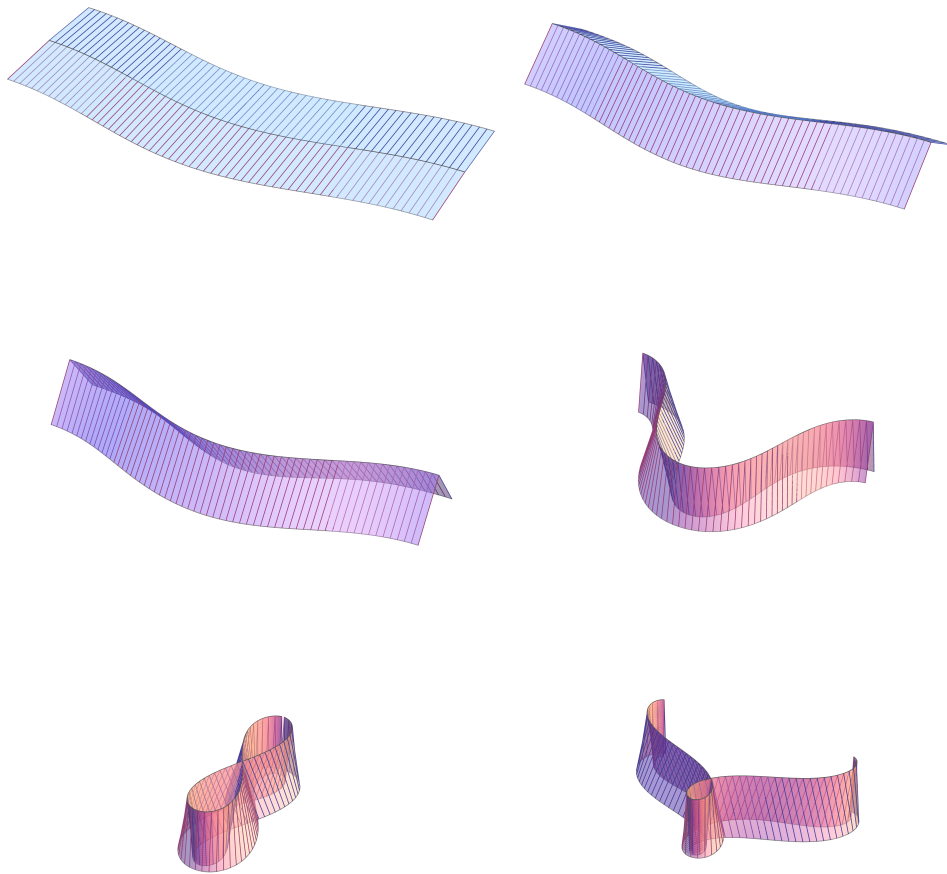


Figure 2.1: planar folds of example (a) with initial values $\varphi(0) = \{0, 0.2\pi, 0.3\pi, 0.45\pi, 0.48\pi, 0.49\pi\}$

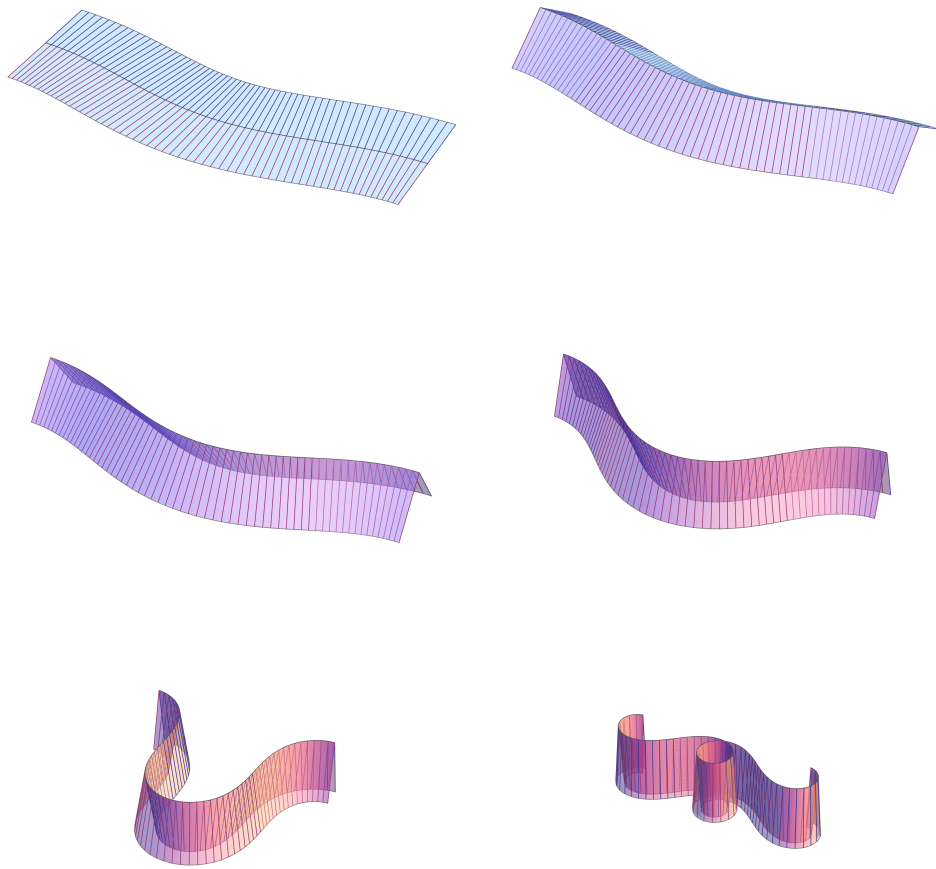


Figure 2.2: planar folds of example (b) with initial values $\varphi(0) = \{0, 0.2\pi, 0.3\pi, 0.4\pi, 0.45\pi, 0.48\pi\}$

Chapter 3

Curved creases of constant angle

Surface curves, whose osculating planes enclose a constant angle with the corresponding tangential planes of a surface are called *pseudo-geodesics*.

Since a curve between two surfaces σ_1 and σ_2 is a curved crease, iff its osculating plane is a bisector of the resp. tangent planes, the investigation of curved creases of constant angle is equivalent to the search for a common pseudo-geodesic of two surfaces w.r.t. the same angle (up to sign).

In this chapter, curved creases of constant angle between cylinders or cones, i.e. the pseudo-geodesics on cylinders and cones, will be studied. On the one hand, they will be characterized in a geometric way as in [20] and [19]. On the other, an analytical approach will prepare parametrizations that are convenient for development. If such a pseudo-geodesic on a cylinder or cone σ is found, the second surface of the crease is the envelope of the tangential planes of σ_1 reflected at the osculating planes of the crease curve. Especially curved creases on cylinders and cones of revolution admit a nice interpretation in terms of catenaries on those surfaces.

In particular, a characterization of curved creases between the surface combinations (cylinder, cylinder), (cylinder, cone) and (cone, cone), also referred to as *bi-cylindrical*, *cylindro-conical* resp. *bi-conical* creases, in terms of geodesics on planes and quadrics can be obtained as a special case of Wunderlich's results in [21] and [22].

The preparations in the first section yield that a curve c on σ_1 is a pseudo-geodesic with enclosing angle φ , iff the Darboux frame of c w.r.t. σ_1 with the curvatures $\kappa_d = \kappa_{g_1}, \kappa_{n_1}$ and geodesic torsion τ_1 , is related to the main

frame of c with curvature κ and torsion τ by

$$\begin{aligned}\kappa_d &= -\kappa \cos \varphi, \\ \kappa_{n_1} &= -\kappa \sin \varphi, \\ \tau_1 &= \tau.\end{aligned}$$

Hence, the *pseudo-geodesic condition* for $\varphi = \text{const} \neq 0$ reads

$$\kappa_d = \kappa_{n_1} \cot \varphi. \quad (3.1)$$

The special case of $\varphi = \frac{\pi}{2}$ yields the well known condition for geodesic curves, i.e. vanishing geodesic curvature.

In the following sections, we will therefore study curves on cylinders and cones that satisfy (3.1) for $\varphi = \text{const} \neq 0 \pmod{\frac{\pi}{2}}$.

3.1 Curved creases of constant angle on cylinders

3.1.1 Geometric approach

The constant angle between the osculating and tangent planes is reflected in the behaviour of the tangents of c , as described in [21], in the following way:

Let σ be a cylinder with z -parallel rulings and tangent planes τ , and c a pseudo-geodesic w.r.t. the angle φ on σ with osculating planes ω . Denote τ° resp. ω° the set of planes that are parallel to τ resp. ω and contain the origin o . Then ω° envelop a cone Λ with vertex o , whose tangent planes ω° enclose constant angle φ with the corresponding planes from the pencil τ° of planes containing the z -axis. Therefore, the intersection of Λ with a sphere with center o is a loxodrome. Since the tangents of c are $\tau \cap \omega$ and thus parallel to the rulings $\tau^\circ \cap \omega^\circ$ of Λ , we conclude the following

Theorem 3.1. *The spherical tangential image of a pseudo-geodesic w.r.t. the angle φ on a cylinder is a spherical loxodrome. The constant angle between the arcs of longitude and the loxodrome is φ .*

3.1.2 Analytic approach

Let σ_1 be a cylinder parametrized with

$$\sigma_1(u, v) = p(u) + v(0, 0, 1)^t \quad (3.2)$$

with $p = (p_1(u), p_2(u), 0)^t \in (0, 0, 1)^\perp$ and, w.l.o.g., $|p'|^2 = p_1'^2 + p_2'^2 = 1$.

Then, σ_1 can be developed into the plane parametrized by $\bar{\sigma}_1 = (u, v, 0)^t$ since the first fundamental forms I and \bar{I} of σ_1 resp. $\bar{\sigma}_1$ read

$$I = \bar{I} = \begin{pmatrix} 1 & 0 \\ 0 & 1 \end{pmatrix}.$$

Denoting $e_3 = (0, 0, 1)^t$, let

$$c(u) = p(u) + h(u)e_3 = (p_1(u), p_2(u), h(u))^t$$

be a parametrization of the crease curve and

$$\bar{c}(u) = (u, h(u))$$

its development in $\bar{\sigma}$.

The curvature κ_p of the planar curve p reads

$$\kappa_p = p'_1 p''_2 - p''_1 p'_2.$$

The tangent t of c reads

$$t = \frac{c'}{|c'|} = \frac{1}{\sqrt{1+h'^2}}(p' + h'e_3).$$

and the remaining vectors of the Darboux frame of c w.r.t. n_1 are

$$n_1 = \frac{(\sigma_1)_u \times (\sigma_1)_v}{|(\sigma_1)_u \times (\sigma_1)_v|} = p' \times e_3 = (p'_2, -p'_1, 0)^t$$

and

$$b_1 = t \times n_1 = \frac{1}{\sqrt{1+h'^2}}(h'p' - e_3).$$

The derivatives of t and n_1 ,

$$t' = \frac{1}{\sqrt{1+h'^2}^3}(-h'h''p' + (1+h'^2)p'' + h''e_3)$$

and

$$n'_1 = p'' \times e_3 = (p''_2, -p''_1, 0)^t,$$

yield the curvatures and torsion of the frame

$$\begin{aligned} \kappa_{n_1} &= \frac{1}{|c'|} t' n_1 = -\frac{1}{1+h'^2} \kappa_p \\ \kappa_d &= -\frac{1}{|c'|} t' b_1 = \frac{h''}{\sqrt{1+h'^2}^3} \\ \tau_1 &= \frac{1}{|c'|} n'_1 b_1 = \frac{h'}{1+h'^2} \kappa_p. \end{aligned}$$

Hence, the pseudo-geodesic condition (3.1) reads

$$\kappa_p = -\frac{h''}{\sqrt{1+h'^2}} \tan \varphi. \quad (3.3)$$

Denoting $\alpha = -\int \kappa_p dt$, integration yields for constant φ

$$\operatorname{arcsinh} h' = \alpha \cot \varphi \quad \implies \quad h' = \sinh(\alpha \cot \varphi). \quad (3.4)$$

Since $c' = (p'_1, p'_2, h')^t$ with $|c'| = \cosh(\alpha \cot \varphi)$, the normalized tangent reads

$$t = \frac{c'}{|c'|} = \frac{1}{\cosh(\alpha \cot \varphi)} \begin{pmatrix} \sin \alpha \\ \cos \alpha \\ \sinh(\alpha \cot \varphi) \end{pmatrix},$$

which is a parametrization of a spherical loxodrome. This confirms Thm. 3.1.

We note, that h can be obtained from a given p by

$$h = \int \sinh(\alpha \cot \varphi) ds.$$

On the other hand, the profile curve p is determined by h through

$$p = \int (\sin \alpha, \cos \alpha) ds \quad \text{with} \quad \alpha = \tan \varphi \operatorname{arcsinh} h' = -\int \kappa_p dt$$

up to Euclidean displacement in the xy -plane.

Unfortunately, the required arc-length parametrization of p in the first case is not satisfactory for applied purposes.

3.1.3 Curved creases of constant angle on cylinders of revolution

In case of a rotational cylinder with radius 1 and the z -axis as axis of revolution, $\alpha(u) = u$ and therefore integration of (3.4) yields

$$h(u) = \tan \varphi \cosh(u \cot \varphi).$$

Since the development of the curve is a parametrization of a *catenary*, it is not surprising that these curves describe the behaviour of chains, i.e. one-dimensional, flexible, inductile objects with an even distribution of mass, when wound around a cylinder, see fig. 3.1.

3.2 Curved creases of constant angle on cones

3.2.1 Geometric approach

Like in the geometric characterization of pseudo-geodesics on cylinders, it is not surprising that we can establish a relation between pseudo-geodesics on cones and loxodromes as well:

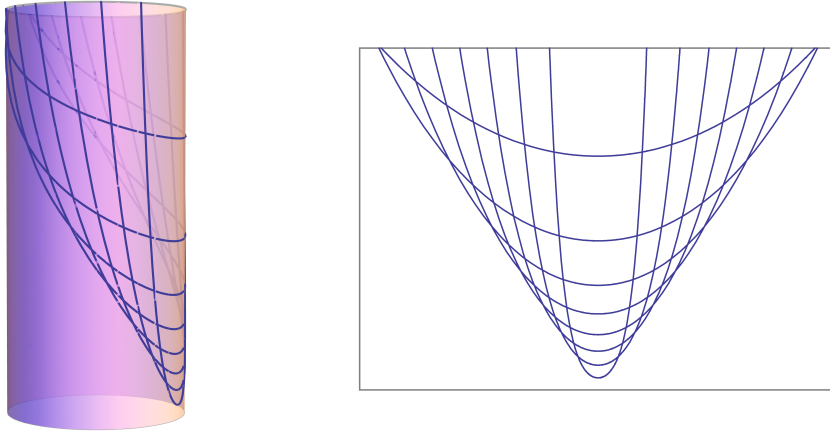


Figure 3.1: cylindrical catenaries and their development

Let σ be a cone with vertex o , c a pseudo-geodesic w.r.t. the angle φ on σ and ρ the polarity of a sphere with center o . Let furthermore τ denote the tangent planes of σ , and ω the osculating planes of c , see fig. 3.2. Then the dual curve of c w.r.t. ρ is traced out by the points ω^ρ and has the tangents $t^\rho = (\omega \cap \tau)^\rho = \omega^\rho \tau^\rho$. Since $o\omega^\rho \perp \omega$ and $o\tau^\rho \perp \tau$, it follows that

$$\varphi = \angle(\omega, \tau) = \angle(o\omega^\rho, o\tau^\rho) = \angle(o\omega^\rho, \omega^\rho \tau^\rho) = \angle(o\omega^\rho, t^\rho).$$

Thus the tangents t^ρ enclose a constant angle with the rulings of the cone $o\omega^\rho$ and the dual curve of c is therefore a loxodrome on $o\omega^\rho$.

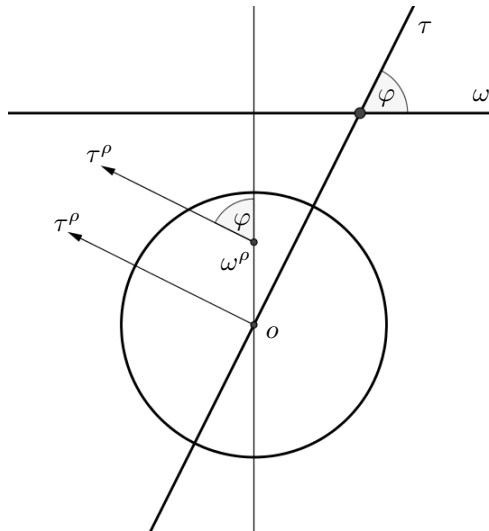


Figure 3.2: illustration of the polarity of Thm. 3.2

Since the argumentation above can be reversed, it follows:

Theorem 3.2. [19, Thm. 3] Let c denote a curve on a cone σ with vertex o and ρ the polarity of a sphere with center o . Then c is a pseudo-geodesic on σ iff the dual curve of c w.r.t. ρ is a loxodrome on a cone with vertex o .

3.2.2 Analytic approach

Let σ_1 be a cone parametrized by

$$\sigma_1(u, v) = vr(u)$$

with $r = (r_1(u), r_2(u), r_3(u))^t$ and, w.l.o.g., $|r| = 1$ and $|r'| = 1$.

Then, σ_1 can be developed in the plane parametrized by $\bar{\sigma}_1 = v(\cos(u), \sin(u), 0)^t$ since the first fundamental forms I and \bar{I} of σ_1 resp. $\bar{\sigma}_1$ read

$$I = \bar{I} = \begin{pmatrix} v^2 & 0 \\ 0 & 1 \end{pmatrix}.$$

Let

$$c(u) = h(u)r(u)$$

be a parametrization of the crease curve and

$$\bar{c}(u) = h(u)\bar{r}(u)$$

with $\bar{r}(u) = (\cos(u), \sin(u))^t$ its development in $\bar{\sigma}$. Then the tangent t of c reads

$$t = \frac{c'}{|c'|} = \frac{1}{\sqrt{h^2 + h'^2}}(h'r + hr').$$

The frame of c w.r.t. σ_1 is completed with the normal vector

$$n_1 = \frac{(\sigma_1)_u \times (\sigma_1)_v}{|(\sigma_1)_u \times (\sigma_1)_v|} = -r \times r'$$

and the bi-normal vector

$$b_1 = t \times n_1 = \frac{1}{\sqrt{h^2 + h'^2}}(-hr + h'r').$$

Let furthermore $\kappa_g^{(r)}$, $\kappa_n^{(r)}$ and $\tau^{(r)}$ denote the quantities of the Frenet frame of r w.r.t. S^2 , that is $(t^{(r)}, n^{(r)}, b^{(r)}) = (r', r, r' \times r)$. They read

$$\begin{aligned} \kappa_n^{(r)} &= r''r &= -1 \\ \kappa_g^{(r)} &= -r''(r' \times r) &= r''(r \times r) \\ \tau^{(r)} &= 0 \end{aligned} \tag{3.5}$$

Computation of the derivatives

$$t' = \frac{1}{\sqrt{h^2 + h'^2}^3}((h^2 - hh'' + 2h'^2)(-rh + r'h') + h(h^2 + h'^2)\kappa_g^{(r)}(r \times r'))$$

and

$$n'_1 = r'' \times r.$$

yields the curvatures and torsion of the frame

$$\begin{aligned} \kappa_{n_1} &= \frac{1}{|c'|} t' n_1 = -\frac{h}{h^2+h'^2} \kappa_g^{(r)} \\ \kappa_d &= -\frac{1}{|c'|} t' b_1 = -\frac{1}{\sqrt{h^2+h'^2}^3} (h^2 - hh'' + 2h'^2) \\ \tau_1 &= \frac{1}{|c'|} n'_1 b_1 = \frac{h'}{h^2+h'^2} \kappa_g^{(r)}. \end{aligned}$$

Hence, the pseudo-geodesic condition (3.1) reads

$$\kappa_g^{(r)} = \frac{h^2 - hh'' + 2h'^2}{h\sqrt{h^2+h'^2}} \tan \varphi. \quad (3.6)$$

If r is parametrized with the angular functions $\eta(u)$ and $\theta(u)$ by

$$r(u) = \begin{pmatrix} \cos \eta \cos \theta \\ \sin \eta \cos \theta \\ \sin \theta \end{pmatrix}$$

the condition $|r'|^2 = 1$ reads

$$\eta'^2 = \frac{1 - \theta'^2}{\cos^2 \theta} \quad \text{for } \theta \neq \frac{\pi}{2} \pmod{\pi}$$

since

$$r' = \eta' \begin{pmatrix} -\sin \eta \cos \theta \\ \cos \eta \cos \theta \\ 0 \end{pmatrix} + \theta' \begin{pmatrix} -\cos \eta \sin \theta \\ -\sin \eta \sin \theta \\ \cos \theta \end{pmatrix}.$$

Then, the geodesic curvature simplifies to

$$\kappa_g^{(r)} = r''(r \times r') = \frac{(1 - \theta'^2) \tan \theta + \theta''}{\sqrt{1 - \theta'^2}}.$$

3.2.3 Curved creases of constant angle on cones of revolution

Specializing the considerations from section 3.2.1 to cones of revolution yields a classification and explicit parametrizations:

Since $t \subset \omega$, it follows that the tangents of the dual curve t^ρ contain the ideal points ω^ρ . If σ is a cone of revolution with opening angle 2α and w.l.o.g. axis z , then the dual surface of σ is the ideal curve of the orthogonal cone of σ . Thus, t^ρ have constant inclination α w.r.t. horizontal planes. If c is a pseudo-geodesic, it follows from Thm. 3.2 that the dual tangents t^ρ enclose constant angle φ with the rulings of the cone ω^ρ . Hence we conclude, that the distance h_ρ from the origin and height z_ρ of the points of the dual curve

of c depend linearly on an arc-length s . We therefore make the following ansatz:

$$h_\rho = s \cos \varphi \quad \text{and} \quad z_\rho = s \sin \alpha + d.$$

The resulting relation

$$\frac{h_\rho}{z_\rho - d} = \frac{\cos \varphi}{\sin \alpha} = \varepsilon = \text{const} \quad (3.7)$$

characterizes a second-order surface of revolution Δ as the set of points, whose distances between a focal point o and the director plane $z = d$ have constant ratio, namely the numerical eccentricity ε . Hence the dual curve of c is a curve of constant slope α on Δ .

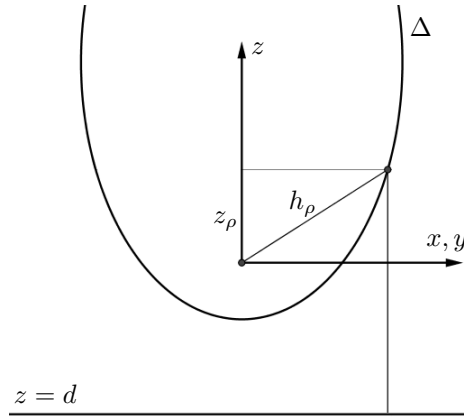


Figure 3.3: illustration of the geometric relation (3.7)

Since the argumentation can be reversed, it follows:

Theorem 3.3. [19, Thm. 4] *Let Δ denote a second-order surface of revolution with vertical axis and real valued numerical eccentricity ε and ρ the polarity on a sphere with a focal point of Δ as center. Applying ρ to a curve of constant slope α on Δ yields a pseudo-geodesic c on a cone of revolution σ with opening angle 2α . The angle φ , that is enclosed by the osculating planes of c and the tangent planes of σ , is determined by*

$$\cos \varphi = \varepsilon \sin \alpha.$$

Conversely, every pseudo-geodesic on a cone of revolution can be obtained from such a construction.

We therefore distinguish between the following cases:

- $\varepsilon < 1$ ($\alpha + \varphi > \frac{\pi}{2}$): “elliptic type” – Δ is a prolate ellipsoid,

- $\varepsilon = 1$ ($\alpha + \varphi = \frac{\pi}{2}$): “parabolic type” – Δ is an paraboloid of revolution,
- $\varepsilon > 1$ ($\alpha + \varphi < \frac{\pi}{2}$),

$$\begin{cases} d \neq 0: & \text{“hyperbolic type” – } \Delta \text{ is a two-sheeted hyperboloid,} \\ d = 0: & \text{“conic type” – } \Delta \text{ is a cone of revolution.} \end{cases}$$

Returning to the parametrization, equation (3.3) for a rotational cone with $\theta = \frac{\pi}{2} - \alpha = \text{const}$ reads

$$\frac{h^2 - hh'' + 2h'^2}{h\sqrt{h^2 + h'^2}} = \frac{\tan \theta}{\tan \varphi}. \quad (3.8)$$

Let w.l.o.g. $\varphi \in (0, \pi)$ and $\theta \in (0, \frac{\pi}{2})$. This yields

$$1 \gtrless \varepsilon \iff \alpha + \gamma \gtrless \frac{\pi}{2} \iff \varphi \gtrless \beta \iff 1 \gtrless \frac{\tan \theta}{\tan \varphi}.$$

With the abbreviations $p = \tan \varphi$ and $q = \tan \theta$, the corresponding solutions of (3.8) finally read

$$h(u) = \begin{cases} \frac{\sqrt{p^2 - q^2}}{p \cos(u\sqrt{p^2 - q^2}/p) + q} & \text{for } \varphi > \theta \dots \text{ elliptic type,} \\ \frac{2q}{u^2 - 1} & \text{for } \varphi = \theta \dots \text{ parabolic type,} \\ \frac{-p^2 + q^2}{p \cosh(u\sqrt{-p^2 + q^2}/p) + q} & \text{for } \varphi < \theta \dots \text{ hyperbolic type } (h'(0) = 0), \\ h_0 e^{u\sqrt{q^2/p^2 - 1}} & \text{for } \varphi < \theta \dots \text{ conic type } (h'(0) \neq 0). \end{cases}$$

Furthermore, the solutions of the initial value problem (3.8) with $h(t_0) = h_0 > 0$ and $h'(t_0) = h_1$ are unique:

Utilizing the substitutions $f_1 = h$ and $f_2 = h'$ yields the equivalent system of differential equations

$$\begin{aligned} f_1' &= g_1(f_1, f_2) = f_2 \\ f_2' &= g_2(f_1, f_2) = \frac{1}{f_1}(f_1^2 + 2f_2^2 - f_1\sqrt{f_1^2 + f_2^2} \frac{\tan \beta}{\tan \varphi}) \end{aligned}$$

with initial values $(f_1(t_0), f_2(t_0)) = (h(t_0), h'(t_0))$. Since $g = (g_1, g_2)$ is Lipschitz-continuous for $f_1 > 0$, the uniqueness of the solution of this initial value problem for $h(t_0) > 0$ follows by Picard-Lindelöf.

As in the case of the cylinder, these curves depict the behaviour of chains wound around a cone of revolution, see fig. 3.4 - 3.7.

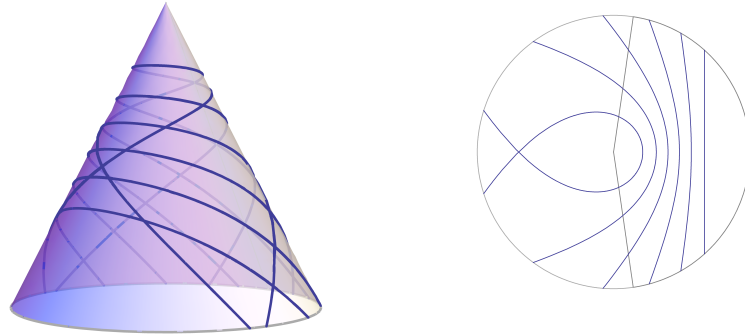


Figure 3.4: conical catenaries of elliptic type and their development

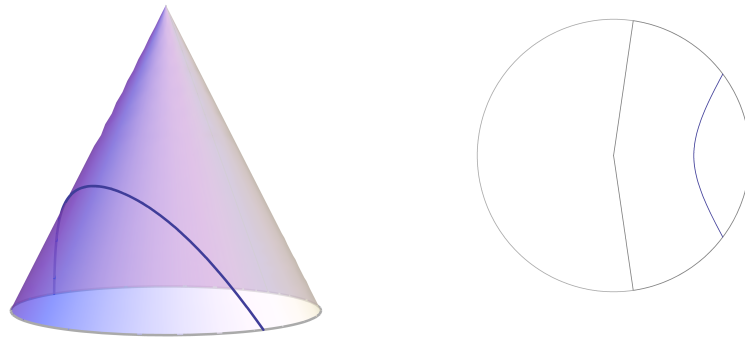


Figure 3.5: a conical catenary of parabolic type and its development

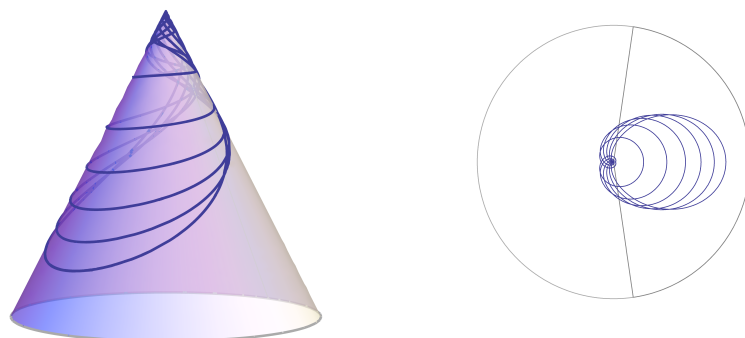


Figure 3.6: conical catenaries of hyperbolic type and their development

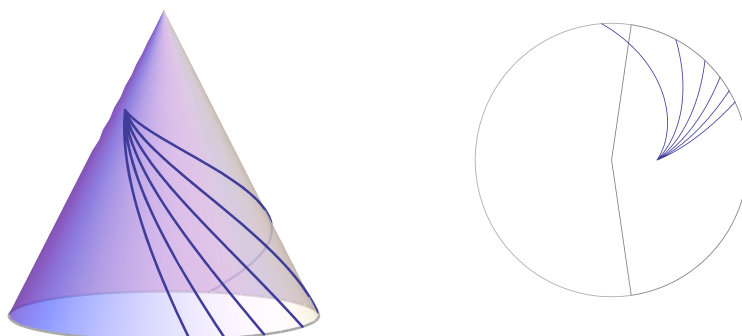


Figure 3.7: conical catenaries of conic type and their development

3.3 Curved creases of constant angle between cylinders and cones

3.3.1 Geometric description

Since the condition for a curved crease of constant angle reads $\psi_1 = \pi - \psi_2$, the developed crease between two families of developed rulings is the curve, for which this reflection property holds. We therefore conclude:

The developed crease between $\left\{ \begin{array}{l} \text{two cylinders is a straight line.} \\ \text{a cylinder and a cone is a parabola.} \\ \text{two cones is an ellipse or a hyperbola.} \end{array} \right.$

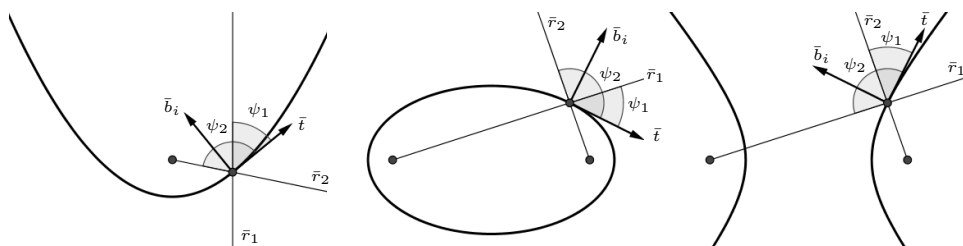


Figure 3.8: illustrations of the developments of crease curves of constant angle between a cylinder and a cone (left) and two cones (middle, right)

Because of the isometry between the spatial configuration and the developed crease, it follows that the curve c must lie on a rotational quadric with one or two real foci. In order to assure the curved crease property, the tangent

planes must be interchanged by the reflection on the osculating planes of c . This yields the following

Theorem 3.4. *A curve c is a curved crease of constant angle between*

1. *two different cylinders, iff c is a geodesic in the plane,*
2. *a cylinder and a cone, iff c is a geodesic on a rotational quadric with one real focal point, i.e. a paraboloid,*
3. *two different cones, iff c is a geodesic on a rotational quadric with two real foci, i.e. a prolate ellipsoid or two-sheeted hyperboloid.*

The real foci of the quadrics are vertices of the resp. cones. In case of the paraboloid, the direction of the axis of rotation corresponds to the direction of the rulings of the cylinder.

Proof. The case of two cylinders is clear from the considerations above.

Let c be a curve on a rotational quadric Ψ with one or two real foci. The tangent t and principal normal n in a curve point p span the osculating plane ω . Furthermore, let r_i denote the normalized vectors from p to the foci of Ψ and $n^\perp = \text{span}\{t, t \times n\}$. Then $\varepsilon = r_1 \cup r_2$ is a plane containing the axis of rotation of Ψ . Let b_i denote the vectors obtained by rotation of t by $\frac{\pi}{2}$ in the planes $t \cup r_i$, so that they lie in the same halfspace bounded by $T_p\Psi$, see fig. 3.9.

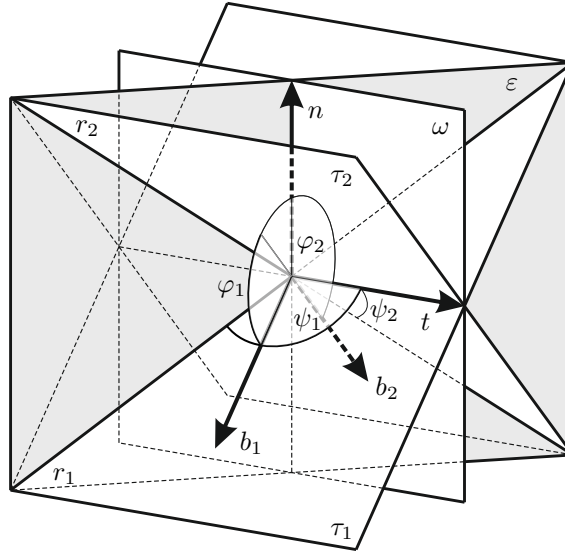


Figure 3.9: the angles and planes used in the proof of Thm. 3.4

Let further the angles ψ_i and φ_i be defined by

$$r_i = \cos \psi_i t + \sin \psi_i b_i \quad \text{and} \quad b_i = \cos \varphi_i n + \sin \varphi_i (t \times n).$$

If $t \in \varepsilon$, then the reflection property of the conic section in $\varepsilon \cap \Psi$ yields $\psi_1 = \pi - \psi_2$. Since $b_1 = b_2$, $\varphi_1 = -\varphi_2 = 0$ if and only if n is perpendicular to $T_p \Psi$.

If $t \notin \varepsilon$, then c is a geodesic on Ψ if and only if $\varepsilon \cap n^\perp = \varepsilon \cap T_p \Psi$ since $t \in n^\perp \cap T_p \Psi$. Because of the reflection property of the conic section $\varepsilon \cap \Psi$, this holds if and only if the reflection on n^\perp maps $r_1 \mapsto -r_2$. This is the case if and only if $\varphi_1 = -\varphi_2$ and $\psi_1 = \pi - \psi_2$. Thus the two sets of rulings r_1 and r_2 define a bi-conical resp. cylindro-conical crease of constant angle.

If on the other hand c is a bi-conical resp. cylindro-conical crease of constant angle, the developed crease curve is a conic section. Due to the isometry between the development and the spatial configuration, c must lie on a rotational quadric Ψ with two foci, which correspond to the vertices of the cones or directions of the rulings resp. \square

In particular, we obtain families of cylindro-conical and bi-conical creases that enclose a constant angle φ , this angle parametrizing the family. The relation between φ and the quantities of the corresponding quadric Ψ can be visualized in the following way:

In case of two real foci, the main axis length of Ψ must equal the main axis length of the corresponding conic section due to the isometry between the spatial configuration and its development. Imagine two pencils of lines in the plane, which are paired so that the reflection property holds, i.e. along an ellipse or a hyperbola, and each two rulings are connected with a joint at their intersection. The family of curved creases of constant angle φ can be generated from this planar configuration, i.e. $\varphi = 0$, by increasing φ in the following way:

In the case of an ellipse, we move the cone vertices apart from each other to induce folds with increasing φ . By increasing distance, i.e. increasing eccentricity of Ψ , the minor axis length decreases.

In case of a hyperbola, we move the cone vertices towards each other to induce folds with increasing φ . As the eccentricity of Ψ decreases, the minor axis length decreases as well.

This behaviour is illustrated in fig. 3.10, fig. 3.15 and fig. 3.16.

Similar considerations can also be done for the case of a paraboloid. We start with two bundles of lines, such that one vertex is at infinity and one a real point. We imagine them again to be paired, so that the reflection property holds, i.e. along a parabola, and connected with a joint at their intersection. Inducing the fold by moving the vertex of the cone, we obtain a one-parameter family of cylindro-conical crease curves on rotational paraboloids.

As φ increases, the focal length of the corresponding paraboloids decreases, see fig. 3.11 and fig. 3.14.

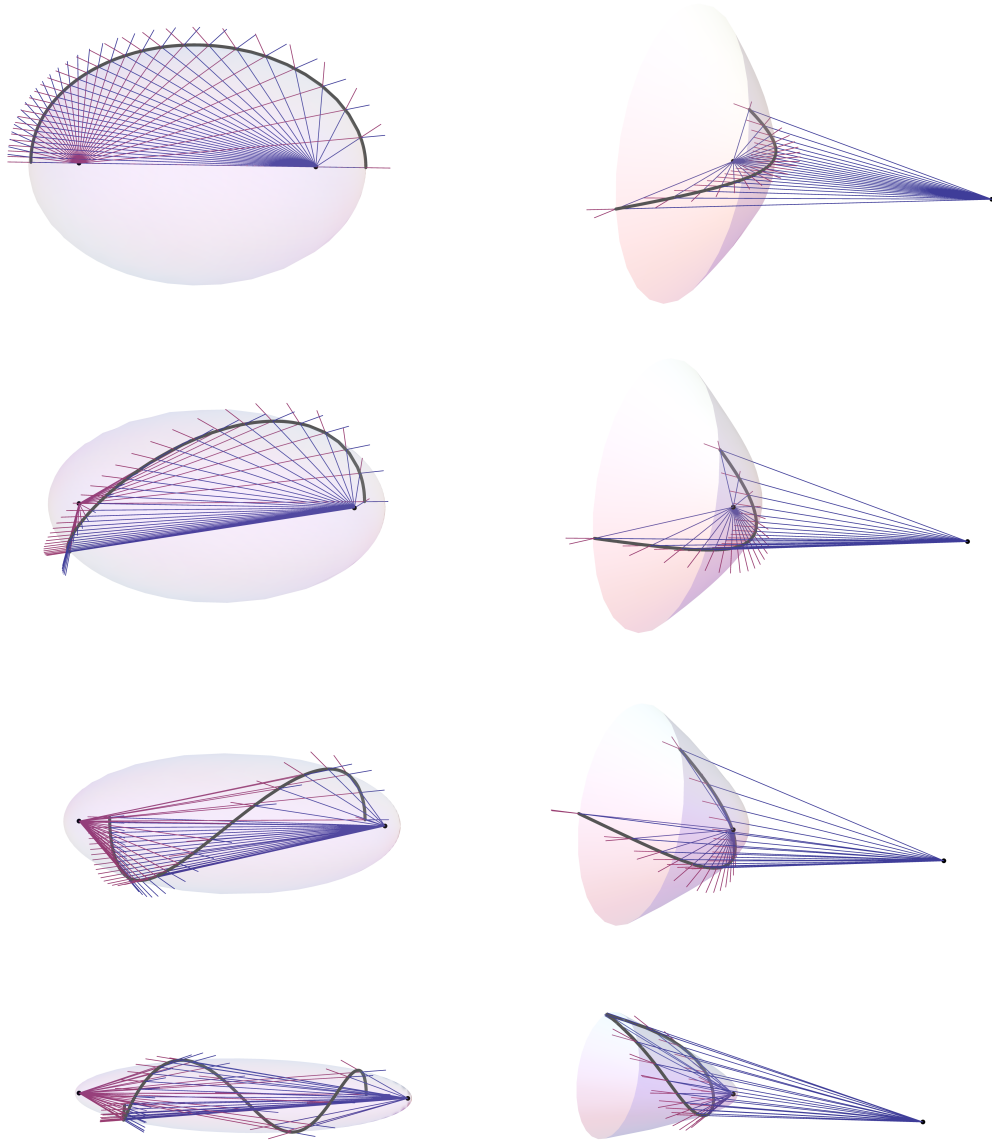


Figure 3.10: rulings of bi-conical creases of constant angle on prolate ellipsoids (left) and two-sheeted hyperboloids (right) with $\varphi \in \{0, 0.2\pi, 0.3\pi, 0.4\pi\}$

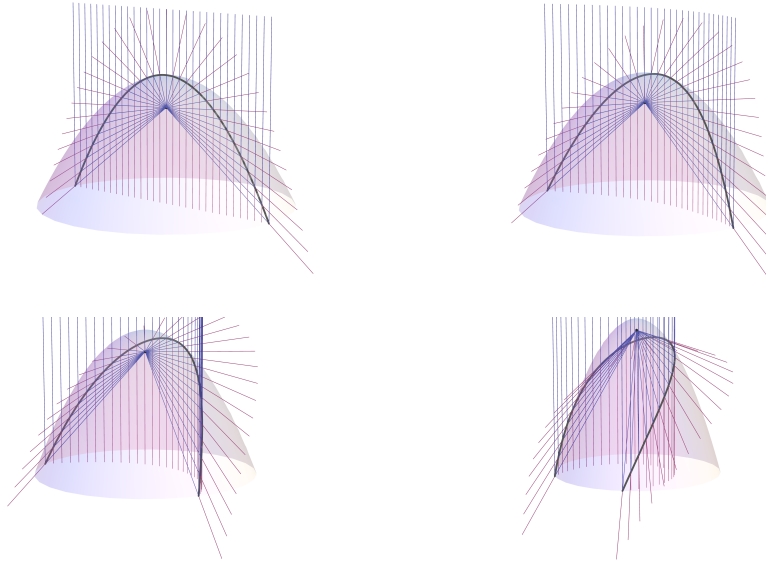


Figure 3.11: rulings of a cylindro-conical crease of constant angle on a paraboloid with $\varphi \in \{0, 0.1\pi, 0.2\pi, 0.3\pi\}$

3.3.2 Other interpretations

Thm. 3.4 is actually a special case of Wunderlich's results in [21] and [22], where he characterizes cylindro-conical and bi-conical pseudo-geodesics. In this section, we give an insight to his geometric approaches.

Pseudo-geodesics between two cylinders

Since the spherical image of the tangents of a pseudo-geodesic on a cylinder is a loxodrome and the direction of the rulings is determined by the pole of the supporting sphere, there are no pseudo-geodesic curves on two different curved cylinders.

Pseudo-geodesics between a cylinder and a cone

If given a cone Γ with vertex o , Wunderlich refers to the cone with vertex o and rulings perpendicular to the tangent planes of Γ as the *polar cone* Λ of Γ . If c is a curve on Λ and ρ the polarity of a sphere with center o , then the tangents of the dual curve of c are parallel to the corresponding rulings of Γ . Together with Thm. 3.1 and Thm. 3.2, we deduce the following construction of cylindro-conical pseudo-geodesics w.r.t. the angles φ_1 and φ_2 :

- start with a spherical loxodrome k with inclination angle φ_1
- determine the polar cone Λ of the cone connecting the origin o with k
- draw a loxodrome l with inclination angle φ_2 on Λ

Then, the dual curve of l w.r.t. a polarity of a sphere with center o is the common pseudo-geodesic.

Wunderlich utilizes this construction to obtain analytical representations and concludes:

Theorem 3.5. [21, Thm. 7] *Every cylindro-conical pseudo-geodesic is also a pseudo-geodesic of a rotational surface Ψ . The axis of Ψ contains the vertex of the cone and its direction corresponds to the direction of the rulings of the cylinder. The meridian curve is the polar curve of a Clairaut multiplicatrix¹ w.r.t. a concentric circle. Furthermore, the sum of the inclination angles of the three osculating planes equals $\frac{\pi}{2}$ (after appropriate determination of sign).*

In case of a curved crease, that is in Wunderlich's notation a pseudo-geodesic w.r.t. the angles γ_1 and $\gamma_2 = -\gamma_1$, the meridian curve simplifies to a bundle of circles containing the origin o ,

$$x^2 + y^2 + z^2 = Cz, \quad (3.9)$$

that is a parabolic pencil of circles. Therefore, the application of the polarity yields a pencil of parabolas with common focal point o and thus the surfaces Ψ are paraboloids. Since the inclination angle of the osculating plane w.r.t. Ψ is $\frac{\pi}{2}$, the common pseudo-geodesic is a geodesic on Ψ .

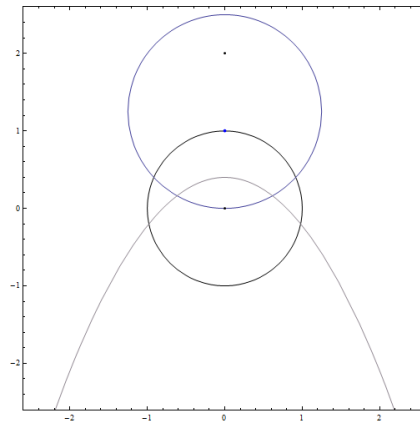


Figure 3.12: the polarity of the unit circle applied to a circle from the parabolic pencil (3.9)

¹see [12], p. 369ff

Furthermore, the intersection curves of the cylindrical surface with planes perpendicular to its rulings are *hypercycloids*² and can be parametrized by

$$\begin{aligned} p_1(\phi) &= \sin(2\gamma_1)(\cosh(c\phi) \cos \phi - c \sinh(c\phi) \sin \phi) \\ p_2(\phi) &= \sin(2\gamma_1)(\cosh(c\phi) \sin \phi + c \sinh(c\phi) \cos \phi) \end{aligned}$$

with $c = \cot \gamma_1$.

The parametrization in (3.12) differs, since the curve is arc-length parametrized there.

Pseudo-geodesics between two cones

It follows from Thm. 3.2 that a bi-conical pseudo-geodesic c is the polar curve of two different cone loxodromes. Polarization of an osculating plane of c on two spheres with centers o_1 resp. o_2 yields two loxodromes l_1 and l_2 whose rulings are parallel. Translating l_2 by $o_1 - o_2$ yields a loxodrome l'_2 on the cone $o_1 l_1$, which is the image of l_2 w.r.t. a collineation κ . This collineation κ is perspective, since the plane orthogonal to $o_1 o_2$ through o_1 is its axis and o_1 its center. Therefore the question about the existence of bi-conical pseudo-geodesics reduces itself to the determination of pairs of loxodromes l_1, l'_2 w.r.t. a bundle in o_1 , so that $l_1^\kappa = l'_2$ for a perspective collineation κ with center o_1 .

It turns out, that these loxodromes lie on one-parameter family of surfaces of revolution. Further investigations and reversing the polarity yields:

Theorem 3.6. *[19, Thm. 6] Every bi-conical pseudo-geodesic is also a pseudo-geodesic curve of a surface of revolution Ψ . The axis connects the vertices of the two cones and the sum of the inclination angles of the osculating plane w.r.t. the surfaces equals $\frac{\pi}{2}$.*

In case of a curved crease, that is in Wunderlich's notation a pseudo-geodesic w.r.t. the angles γ_1 and $\gamma_2 = -\gamma_1$, the surfaces of revolution containing the loxodromes are spheres of the hyperbolic sphere pencil with nullspheres $(0, 0, 0)$ and $(0, 0, 2)$

$$x^2 + y^2 + z^2 = C^2(z - 1). \quad (3.10)$$

Applying the polarity of the unit-sphere with the origin o_1 as center yields a pencil of second order surfaces of revolution with common focal points o_1 and $(0, 0, 1)$.

²see [13], p. 121ff

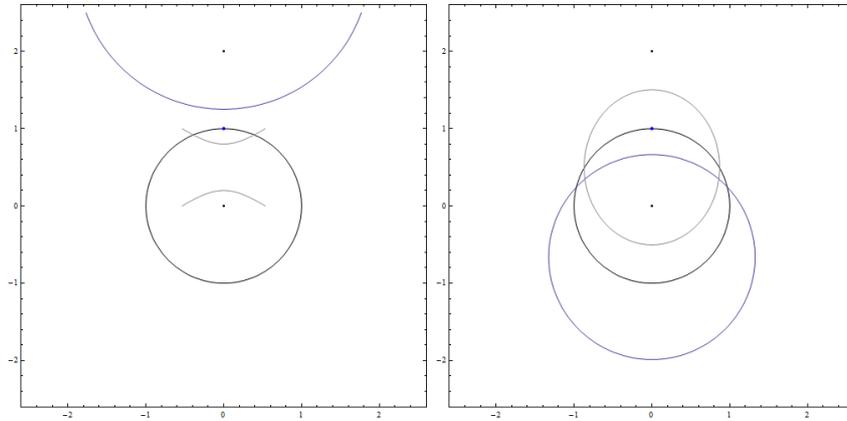


Figure 3.13: circles of the “lower” and “upper” half of a hyperbolic pencil (3.10) polarized on the unit circle

Furthermore, Wunderlich concludes:

Theorem 3.7. [22, Thm. 10] *The geodesic lines c of a second order surface of revolution with focal points f_1 and f_2 are the pseudo-geodesics on the cones f_1c and f_2c .*

3.3.3 Analytic description

Developed rulings \bar{r}_2 of σ_2 if σ_1 is a cylinder

From the formulas above, the angle ψ_1 between the tangent and the ruling is determined by

$$\cot \psi_1 = \frac{\tau_1}{\kappa_{n_1}} = -h'.$$

Therefore, we write

$$\cos \psi_1 = \frac{h'}{\sqrt{1+h'^2}} \quad \text{and} \quad \sin \psi_1 = -\frac{1}{\sqrt{1+h'^2}}.$$

The tangent \bar{t} and normal vector \bar{n} of the developed curve $\bar{c} = (u, h(u))$ read

$$\bar{t} = \frac{1}{1+h'^2}(1, h') \quad \text{and} \quad \bar{n} = \frac{1}{1+h'^2}(-h', 1).$$

Since $\varphi = \text{const}$, iff $\psi_2 = \pi - \psi_1$, the rulings of $\bar{\sigma}_2$ are

$$\bar{r}_2 = \cos \psi_2 \bar{t} + \sin \psi_2 \bar{n} = \frac{1}{1+h'^2}(2h', h'^2 - 1). \quad (3.11)$$

Curved creases of constant angle between two cylinders

The second surface σ_2 is a cylinder, if the developed rulings are parallel, that is, if there is a unit-vector $v = (v_1, v_2)$, so that

$$\bar{r}_2 = (v_1, v_2) \implies h' = \pm \sqrt{\frac{1+v_2}{1-v_2}}.$$

Therefore,

$$h(u) = \pm \sqrt{\frac{1+v_2}{1-v_2}} u + c_1$$

and thus $\kappa_d \equiv 0$. Therefore the curvature κ must vanish if the crease is not a complete fold.

Curved creases of constant angle between a cylinder and a cone

The second surface σ_2 is a cone, if the developed rulings \bar{r}_2 are a bundle of lines with a real vertex. Thus the developed vertex $\bar{z} = (\bar{z}_1, \bar{z}_2)$ is contained in all rulings, iff

$$\bar{r}_2^\perp \bar{z} = \bar{r}_2^\perp \bar{c} \iff (h'^2 - 1)\bar{z}_1 - 2h'\bar{z}_2 = (h'^2 - 1)u - 2h'h$$

holds for all parameter values of u .

In case of $\bar{z}_1 = 0$, the differential equation reads

$$-2h'z_2 = (h'^2 - 1)u - 2h'h$$

and is solved by the two parabolas

$$h_{1,2}(u) = \frac{1}{2}(2z_2 \mp \frac{1}{c}u^2 \pm c) \quad \text{with } c \geq 0,$$

as already proposed in the previous section. In case of $\bar{z}_1 \neq 0$, the solution parabola of $(0, \bar{z}_2)$ has to be translated by $(\bar{z}_1, 0)$, which yields the solutions

$$h_{1,2}(u) = \frac{1}{2}(2z_2 \mp c(u - z_1)^2 \pm \frac{1}{c}) \quad \text{with } c \geq 0.$$

Furthermore, the height-function h also determines the profile curve p of the cylinder σ_1 . Since the developed crease can be translated to the origin, we assume w.l.o.g. h to be

$$h(u) = cu^2.$$

Equation (3.3) yields the curvature of the profile curve

$$\kappa_p(s) = -\frac{2c}{\sqrt{1+4c^2s^2}} \tan \varphi$$

and thus angular function $\alpha = -\int \kappa_p$ reads

$$\alpha(u) = -\operatorname{arcsinh}(2cu) \tan \varphi.$$

Integration of (3.4) results in the parametrization of the profile curve

$$p_1(u) = u \cos^2 \varphi \cos \alpha - \frac{\sqrt{1+4c^2u^2} \sin(2\varphi)}{4c} \sin \alpha \quad (3.12)$$

$$p_2(u) = 4cu \cos^2 \varphi \sin \alpha + \frac{\sqrt{1+4c^2u^2} \sin(2\varphi)}{4c} \cos \alpha - \frac{\sin(2\varphi)}{4c}. \quad (3.13)$$

Solving $r_2 \times (c - z) = 0$ yields the vertex

$$z = \left(0, -\frac{\sin(2\varphi)}{4c}, \frac{\cos(2\varphi)}{4c}\right)_t$$

of the cone, which is also the focal point of the paraboloid, see fig. 3.14.

Developed rulings \bar{r}_2 of σ_2 if σ_1 is a cone

From the formulas above, the angle ψ_1 between the tangent and the ruling is determined by

$$\cot \psi_1 = \frac{\tau_1}{\kappa_{n_1}} = -\frac{h'}{h}.$$

Therefore, we write

$$\cos \psi_1 = -\frac{h'}{\sqrt{h^2 + h'^2}} \quad \text{and} \quad \sin \psi_1 = \frac{h}{\sqrt{h^2 + h'^2}}.$$

Denoting $\bar{r} = (\cos u, \sin u)$ and $\bar{r}^\perp = (-\sin u, \cos u)$, the tangent \bar{t} and normal vector \bar{n} of the developed curve $\bar{c} = h\bar{r}$ read

$$\bar{t} = \frac{1}{\sqrt{h^2 + h'^2}}(h'\bar{r} + h\bar{r}^\perp) \quad \text{and} \quad \bar{n} = \frac{1}{\sqrt{h^2 + h'^2}}(-h\bar{r} + h'\bar{r}^\perp),$$

which confirms to

$$\bar{r}_1 = \cos \psi_1 \bar{t} + \sin \psi_1 \bar{n} = \bar{r}.$$

Since $\varphi = \text{const}$, iff $\psi_2 = \pi - \psi_1$, the rulings r_2 of $\bar{\sigma}_2$ are

$$\bar{r}_2 = \cos \psi_2 \bar{t} + \sin \psi_2 \bar{n} = \frac{1}{h^2 + h'^2}((h^2 - h'^2)\bar{r} - 2hh'\bar{r}^\perp). \quad (3.14)$$

Curved creases of constant angle between two cones

Utilizing equation (3.14), the Hesse normal form of the second rulings reads

$$2h^2h = (2hh'\bar{r} + (h^2 - h'^2)\bar{r}^\perp) \begin{pmatrix} x \\ y \end{pmatrix}.$$

W.l.o.g., we assume the vertex z of the second cone to be $(z_1, 0)$, and thus a necessary condition for h reads

$$2h^2h' = (2hh' \cos u - (h^2 - h'^2) \sin u)z_1.$$

Not surprisingly, choosing h to be the “height” for the parametrization of an ellipse with focal points $(0, 0)$ and $(z_1, 0)$ and minor axis length b , that is

$$h_{ell}(u) = \frac{4b^2(\pm\sqrt{4b^2 + z_1^2} + z_1 \cos u)}{8b^2 + (1 - \cos(2u))z_1^2}$$

is a solution of the differential equation above.

Also, h being the “height” for the parametrization of an hyperbola with focal points $(0, 0)$ and $(z_1, 0)$ and minor axis length b , that is

$$h_{hyp}(u) = \frac{4b^2(\pm\sqrt{-4b^2 + z_1^2} + z_1 \cos u)}{8b^2 - (1 - \cos(2u))z_1^2}$$

solves the differential equation.

The functions h_{ell} and h_{hyp} determine the geodesic curvature $\kappa_g^{(r)}$ of the direction vectors of the first cones rulings trough the relation established in (3.6). The illustrations in fig. 3.15 and fig. 3.16 of $c = hr$ were done with numerical integration of the frame of r given in (3.5).

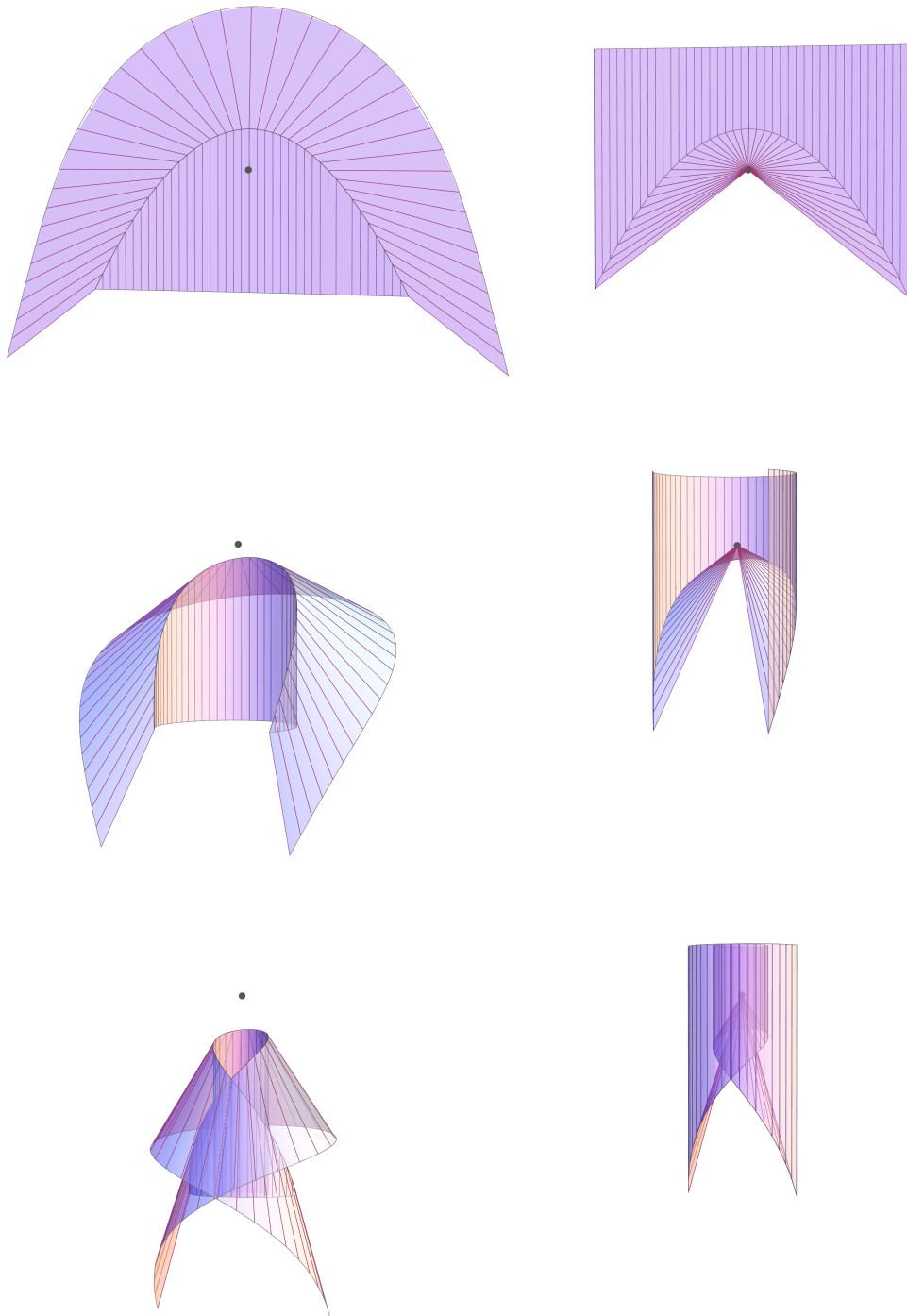


Figure 3.14: cylindro-conical crease of constant angle on a paraboloid with $\varphi \in \{0, 0.3\pi, 0.4\pi\}$

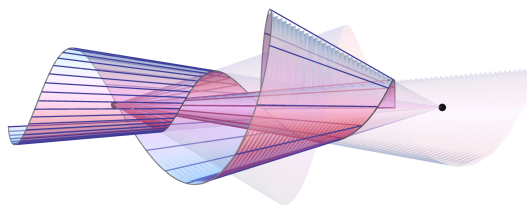
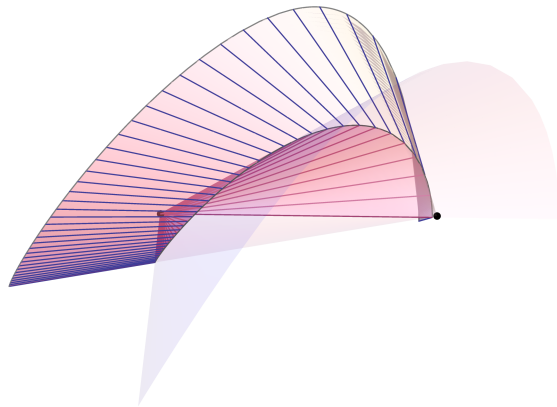
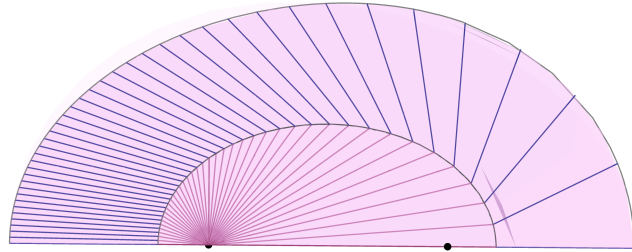


Figure 3.15: bi-conical crease of constant angle on a prolate ellipsoid with $\varphi \in \{0, 0.2\pi, 0.4\pi\}$

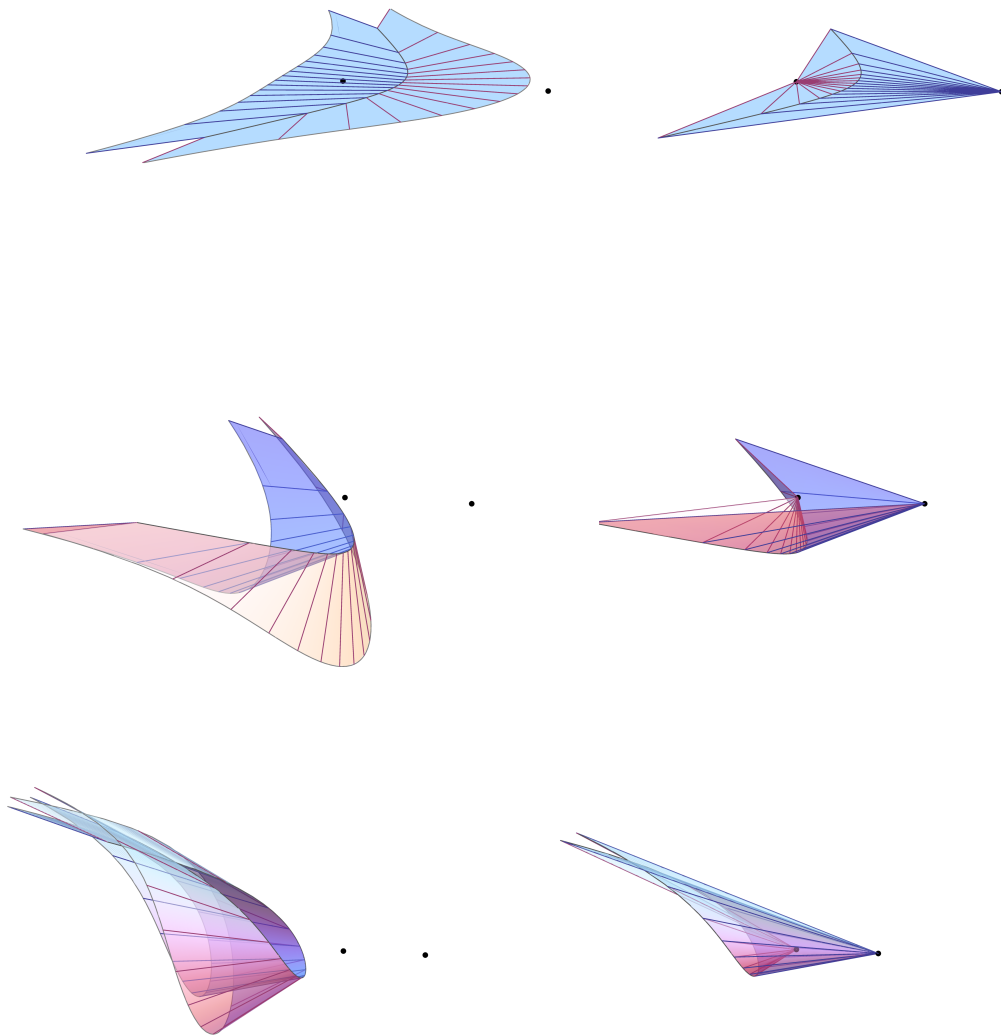


Figure 3.16: bi-conical crease of constant angle on a two-sheeted hyperboloid with $\varphi \in \{0, 0.3\pi, 0.44\pi\}$

Part II

Optimization

Chapter 4

Algorithmic setup

During my employment at *Rechenraum*, a company founded by Dr. Simon Flöry specializing in geometric data processing, I was given the opportunity to develop the mathematical core for a Rhinoceros3D plug-in for the interactive design of developables with curved creases, based on [18]. The following chapters describe the implementation and give examples of its functionality.

4.1 Algorithm

The idea behind the algorithm proposed by Tang et al. is the following: for a set of variables $x \in \mathbb{R}^N$, the *hard constraints*, e.g. the developability condition, are expressed in at most quadratic equations

$$\phi_i(x) = 0, \quad i = 1, \dots, M_1.$$

The resulting system of equations is in general underdetermined and high-dimensional and thus its minimization is not trivial.

The *guided projection approach* of Tang et al. combines an iterative Gauß-Newton algorithm with further, at most quadratic *soft constraints*,

$$\psi_i(x) = 0 \quad i = 1, \dots, M_2,$$

e.g. fairness energies, which lead the interim iterations x_1, x_2, \dots on the solution manifold:

In every iteration x_k , the linearized hard resp. soft constraints read

$$\phi_i(x_k) + \nabla \phi_i(x_k)(x - x_k) = 0 \quad \text{and} \quad \psi_i(x_k) + \nabla \psi_i(x_k)(x - x_k) = 0$$

and can therefore be expressed in the systems of linear equations

$$A_h^{(k)} x - b_h^{(k)} = 0 \quad \text{and} \quad A_s^{(k)} x - b_s^{(k)} = 0.$$

Introducing the weights $\varepsilon_1, \varepsilon_2$ and additionally imposing a *Tychonoff regularization*, the next iterate x_{k+1} is computed as the minimizer of the *weighted linear least squares*

$$\|A_h^{(k)}x - b_h^{(k)}\|^2 + \varepsilon_1^2 \|A_s^{(k)}x - b_s^{(k)}\|^2 + \varepsilon_2^2 \|x - x_k\|^2. \quad (4.1)$$

Tang et al. propose, that ε_1 can be decreased in every iteration to facilitate convergence.

This algorithm terminates if either the maximum number of iterations is exceeded or the maximum relative change of the residual falls below a given threshold.

4.2 Weighted linear least squares

The sum of the linear squares in (4.1) can be written as

$$\|W(Ax - b)\|^2 \quad \text{with} \quad W = \text{diag}(1, \dots, 1, \varepsilon_1, \dots, \varepsilon_1, \varepsilon_2, \dots, \varepsilon_2), \quad (4.2)$$

and expanded to

$$\begin{aligned} \|W(Ax - b)\|^2 &= (W(Ax - b))^t(W(Ax - b)) \\ &= (Ax - b)^t W^2 (Ax - b) \\ &= (Ax)^t W^2 Ax - (Ax)^t W^2 b - b^t W^2 Ax + b^t W^2 b \\ &= x^t A^t W^2 Ax - 2b^t W^2 Ax + b^t W^2 b. \end{aligned}$$

Therefore, minimization of (4.2) results in solving the so-called *normal equations*

$$A^t W^2 Ax - A^t W^2 b = 0,$$

which are obtained from differentiation with respect to x .

4.3 Interactive design

We will see that this iterative algorithm will, if the initialization is good enough, in general reduce the residual strongly in the first iterations, yielding feasible results. The implementation therefore calls a small number of iterations, e.g. 10-20, per intermediate position of a mouse move to give immediate visual feedback to the user. When the mouse is released at the final position, the number of iterations can be increased, e.g. to 100, taking longer computation time into account. In both cases, the second termination condition is set to a low value, e.g. 10^{-7} . As we will see, this condition unfortunately will not be active very often.

Chapter 5

Computational setup

5.1 Theoretical background

We refer to surfaces parametrized by

$$\sigma(u, v) = (1 - v)a(u) + vb(u) \quad \text{with } v \in [0, 1] \quad (5.1)$$

with boundary B-spline curves a and b as *ruled surfaces patches*. We assume a and b to be of the same degree d and defined by the control point sequences a_i and b_j over the same interval $[u_0, u_{end}]$.

The ruled surface patch σ is *developable*, iff

$$p(u) = \det(b(u) - a(u), a'(u), b'(u)) = 0 \quad (5.2)$$

holds for parameters $u \in [u_0, u_{end}]$.

Denoting the four boundaries of a ruled surface patch by s in case of a spline, r in case of a ruling and p , if the corresponding boundary (s or r) degenerates to a point, *developables* are composed of the following types of developable surfaces:

- $srsr$: a regular developable surface patch,
- $srsp$: a developable surface with one boundary ruling degenerated to a point,
- $spsp$: a developable surface with both boundary rulings degenerated to points,
- $srpr$: a cone,
- $r...r$: a planar polygon.

Although a combination of an infinite number of them is theoretically possible, we consider just finite combinations for modelling purposes.

As seen in previous sections, the transition curve a of two surfaces is a curved crease, iff the osculating plane $\text{span}\{t, n\}$ bisects the corresponding tangent planes $\text{span}\{t, b_i\}$. The angle φ of the crease is defined by

$$\cos \varphi = nb_1 = nb_2 \quad \text{and} \quad \sin \varphi = nn_1 = -nn_2, \quad (5.3)$$

and thus the osculating plane is orthogonal to $n_1 + n_2$.

Furthermore, we will introduce a constraint to preserve an approximated isometry between the spatial configuration and a given development.

In conclusion, our computational approach is as follows:

We store the combinatorial information of a composite surface in a mesh, whose faces correspond to surface patches and edges to curved creases or boundaries. We optimize the control points of those curves and auxiliary variables with constraints imposing

- developability on faces,
- the curved crease condition on edges,
- isometry on the whole mesh.

As soft constraints, we will smooth the curves with a fairness energy. In addition to the overall Tychonoff-regularization, we impose further regularizations in order to prevent trivial results.

5.2 Detailed discussion of variables and constraints

When it comes to implementation details, we will denote either of the at most quadratic constraints ϕ_i and ψ_i by $F_{\{cond\}}$, where $\{cond\}$ stands for an abbreviation of the constraint. Therefore, our objective function reads

$$\sum \varepsilon_{\{cond\}}^2 \|F_{\{cond\}}\|^2.$$

We will also give simplified examples for the gradients $\nabla F_{\{cond\}}$.

Furthermore, we write

$$\mathbf{a} = (a_{01}, a_{02}, a_{03}, a_{11}, a_{12}, a_{13}, \dots, a_{n1}, a_{n2}, a_{n3})^t$$

for the vector consisting of triples of coordinates (a_{i1}, a_{i2}, a_{i3}) of the control points a_i .

5.2.1 Developability constraint

Since the boundary curves of a patch are of degree d in the resp. parameter sub-intervals defined by their knot-sequence, we can restrict the developability condition (5.2) to a finite number of evaluation parameters. For a simplified counting of the number of evaluation points, we postulate that a and b have the same number of control points $m + 1$.

If that is the case, p in equation (5.2) is a polynomial of degree at most $3d - 2$ in the corresponding parameter sub-intervals $[u_i, u_{i+1}]$. Since a and b admit the representation

$$a(u) = \sum_{k=0}^d c_{a,k} u^k \quad \text{and} \quad b(u) = \sum_{k=0}^d c_{b,k} u^k \quad \text{for} \quad u \in [u_i, u_{i+1}],$$

p simplifies to

$$p(u) = \sum_{k=0}^d \sum_{l=0}^{d-1} \sum_{j=0}^{d-1} u^{k+l+j} \det(c_{b,k} - c_{a,k}, c_{a,l+1}, c_{b,j+1}).$$

The determinant vanishes for $k = d$ and $d - 1 = l = j$, and thus the polynomial p is of degree at most $3d - 3$. Hence it is sufficient to enforce developability in $3d - 2$ parameter values of each sub-interval.

In order to avoid lengthy formulations, we furthermore assume the two boundary curves of a patch to be defined over the same (uniform) knot-vector. We denote the set of parameters obtained by equidistant division of each sub-interval into $3d - 2$ parameters by P_1 .

Since p is a cubic constraint in the unknown control points, we rewrite the *developability condition*

$$0 = (b - a)n = a'n = b'n,$$

introducing normals n , which are constant along a ruling exactly in case of a developable surface. By adding new variables for the normals n , we turn the cubic constraint into a quadratic one.

5.2.2 Normals as variables

Tang et al. propose two ways how normals can be added to the optimization problem as variables:

Either, the normals are introduced at every evaluation parameter of the developability condition, in the following referred to as *normal vectors*.

Alternatively, it is possible to approximate the spline $a' \times b'$ of degree $2n - 2$ by a *normal spline* of (user-defined) lower degree d_{ns} with a certain number

of control points m_{ns} , which are used as variables. This can reduce the number of variables for normals.

Example: In case of a uniform knot sequence of a spline of degree d with $m+1$ control points, we have $m+1-d$ parameter sub-intervals. Therefore, the number of used normal vectors would be $(m+1-d)(3d-2)$. Therefore, we reduce the dimension of variables of the optimization problem by choosing m_{ns} lower than this value.

Implementation

A B-spline a of degree d can be represented as a linear combination of its control points a_i with the basis functions as coefficients

$$a(u) = \sum_{i=0}^m N_i^d(u) a_i.$$

The l -th derivative w.r.t. the curve parameter u can be then written as

$$a^{(l)}(u) = \sum_{i=0}^m N_i^{d(l)}(u) a_i.$$

Unlike Tang et al., we found it more convenient to use these basis functions for the evaluation of the B-spline curves and its derivatives instead of their de Boor points.

Denoting

$$\mathbf{N}_k^{d,m(l)} = \left(N_0^{d(l)}(u_k) I_3 \quad N_1^{d(l)}(u_k) I_3 \quad \dots \quad N_m^{d(l)}(u_k) I_3 \right)$$

with $I_3 = \text{diag}(1, 1, 1)$, the evaluation of $a^{(l)}$ a parameter $u_k \in P_1$ can then be written as

$$a^{(l)}(u_k) = \mathbf{N}_k^{d,m(l)} \mathbf{a}.$$

Furthermore, the evaluation of $a^{(l)}$ in all parameter values $u_0, u_1, \dots \in P_1$ can be done in a single matrix-vector multiplication

$$\begin{pmatrix} a^{(l)}(u_0) \\ a^{(l)}(u_1) \\ \vdots \end{pmatrix} = \begin{pmatrix} \mathbf{N}_0^{d,m(l)} \\ \mathbf{N}_1^{d,m(l)} \\ \vdots \end{pmatrix} \mathbf{a}.$$

The matrices $\mathbf{N}_k^{d,m(l)}$ can be precomputed as soon as the number of control points and the degree of the B-spline are known and are independent from the positions of the control points. Therefore, they do not change in the

course of the actual optimization, where the B-spline curves need to be evaluated.

The same holds also for the evaluation of the normals with matrices $\mathbf{N}_k^{d_{ns}, m_{ns}(l)}$ if the normal-spline is used.

If the simplified extraction of the vector of variables of our optimization problem reads

$$\mathbf{x} = \begin{pmatrix} \mathbf{a} \\ \mathbf{b} \\ \mathbf{n} \end{pmatrix},$$

the developability condition for a face with boundary curves a , b and normals n can be written as

$$\|F_{dev}(\mathbf{x})\|^2 = \sum_{k=0}^{|P_1|} \|F_{dev,k}(\mathbf{x})\|^2$$

with

$$F_{dev,k} = \begin{pmatrix} (b(u_k) - a(u_k))n(u_k) \\ a'(u_k)n(u_k) \\ b'(u_k)n(u_k) \end{pmatrix} = \begin{pmatrix} \mathbf{n}_k \cdot (\mathbf{N}_k^{d,m}(\mathbf{b} - \mathbf{a})) \\ \mathbf{n}_k \cdot (\mathbf{N}_k^{d,m'}\mathbf{a}) \\ \mathbf{n}_k \cdot (\mathbf{N}_k^{d,m'}\mathbf{b}) \end{pmatrix} \quad \text{for } u_k \in P_1,$$

where

$$\mathbf{n}_k = \begin{cases} (n_{k1}, n_{k2}, n_{k3})^t & \text{normal vectors,} \\ \mathbf{N}_k^{d_{ns}, m_{ns}} \mathbf{n} & \text{normal spline.} \end{cases}$$

The corresponding gradient reads

$$\nabla F_{dev,k} = \begin{pmatrix} -\mathbf{n}_k \cdot \mathbf{N}_k^{d,m} & \mathbf{n}_k \cdot \mathbf{N}_k^{d,m} & (\mathbf{N}_k^{d,m}(\mathbf{b} - \mathbf{a})) \cdot E \\ \mathbf{n}_k \cdot \mathbf{N}_k^{d,m'} & & (\mathbf{N}_k^{d,m'}\mathbf{a}) \cdot E \\ & \mathbf{n}_k \cdot \mathbf{N}_k^{d,m'} & (\mathbf{N}_k^{d,m'}\mathbf{b}) \cdot E \end{pmatrix},$$

with

$$E = \begin{cases} I_3 & \text{normal vectors,} \\ \mathbf{N}_k^{d_{ns}, m_{ns}} & \text{normal spline,} \end{cases}$$

Of course, this representation holds just in case of one patch with unified orientations. As the combinatorics of the problem grow, and if furthermore, control points are multiple or fixed, the indices of the variables are not successive any more and thus attention needs to be paid when it comes to the location of the entries in the Jacobian of the whole problem.

Using derivatives of the curves instead of the de Boor points has the disadvantage of possible high variations of the entries in the Jacobian. In order to avoid big outliers, we therefore scale the three rows of $F_{dev,k}$ and $\nabla F_{dev,k}$ with the *constant* factors $\frac{1}{|b(u_k) - a(u_k)|}$, $\frac{1}{|a'(u_k)|}$ and $\frac{1}{|b'(u_k)|}$ resp.

5.2.3 Unit-length constraint for normals

Since the developability condition is trivially fulfilled if the normals become zero-vectors, an additional constraint for unit-length is needed and reads

$$\sum (n \cdot n - 1)^2.$$

In case of normal vectors, we demand this unit length in every evaluation parameter as a soft constraint with weight ε_{unit}^{nv} . In case of the normal spline, we require unit-length for certain control points of the normal spline, e.g. the first and the last one, as a hard constraint and the other control points to be of unit length as soft constraints with lower weight ε_{unit}^{ns} .

This condition is important since disappearing normals usually go hand in hand with the loss of developability (and the curved crease condition).

Implementation

For $\mathbf{x} = \mathbf{n}$, we write

$$\|F_{unit}(\mathbf{x})\|^2 = \sum_{k=0}^{|P_1|} \|F_{unit,k}(\mathbf{x})\|^2$$

with

$$F_{unit,k}(\mathbf{x}) = (n_{k1}^2 + n_{k2}^2 + n_{k3}^2 - 1).$$

Therefore

$$\nabla F_{unit,k}(\mathbf{x}) = 2(n_{k1}, n_{k2}, n_{k3}).$$

5.2.4 Curved crease condition

Since the osculating plane is in general spanned by a' and a'' , we rewrite (5.3) to obtain the *curved crease* condition for our implementation purposes

$$0 = a'(n_1 + n_2) = a''(n_1 + n_2).$$

The orientation of the normals in this equation is crucial, since a change of sign corresponds to the *geodesic crease* condition

$$0 = a'(n_1 - n_2) = a''(n_1 - n_2),$$

where the curves developed w.r.t. the two surfaces are reflected.

Given a polynomial crease curve on a polynomial surface, the second involved surface is in general not polynomial, see [15]. Therefore, this condition is only an approximation. Another drawback is that this condition performs correctly only if $\|n_1\| = \|n_2\|$, which also is not guaranteed.

Nevertheless, it turns out that we achieve an accuracy that is high enough for our purposes since the used materials are usually forgiving when it comes to small “imperfections”. We therefore enforce the two curved crease conditions at the same parameter values as the developability condition, i.e. P_1 .

Implementation

We illustrate the quadratic constraint $F_{cc}(\mathbf{x})$ for two given patches with boundary curves (a, b) and (a, c) with normals n_1 and n_2 . The extracted necessary variables are

$$\mathbf{x} = \begin{pmatrix} \mathbf{a} \\ \mathbf{b} \\ \mathbf{c} \\ \mathbf{n}_1 \\ \mathbf{n}_2 \end{pmatrix}.$$

Then

$$\|F_{cc}(\mathbf{x})\|^2 = \sum_{k=0}^{|P_1|} \|F_{cc,k}(\mathbf{x})\|^2$$

with

$$F_{cc,k} = \begin{pmatrix} a'(u_k)(n_1(u_k) + n_2(u_k)) \\ a''(u_k)(n_1(u_k) + n_2(u_k)) \end{pmatrix} = \begin{pmatrix} (\mathbf{n}_{1,k} + \mathbf{n}_{2,k}) \cdot (\mathbf{N}_k^{d,m'} \mathbf{a}) \\ (\mathbf{n}_{1,k} + \mathbf{n}_{2,k}) \cdot (\mathbf{N}_k^{d,m''} \mathbf{a}) \end{pmatrix}$$

where

$$\mathbf{n}_{i,k} = \begin{cases} (n_{i,k1}, n_{i,k2}, n_{i,k3})^t & \text{normal vectors,} \\ \mathbf{N}_k^{d_{ns}, m_{ns}} \mathbf{n}_i & \text{normal spline.} \end{cases}$$

Thus the gradient reads

$$\nabla F_{cc,k} = \begin{pmatrix} (\mathbf{n}_{1,k} + \mathbf{n}_{2,k}) \cdot \mathbf{N}_k^{d,m'} & 0 & 0 & (\mathbf{N}_k^{d,m'} \mathbf{a}) \cdot E & (\mathbf{N}_k^{d,m''} \mathbf{a}) \cdot E \\ (\mathbf{n}_{1,k} + \mathbf{n}_{2,k}) \cdot \mathbf{N}_k^{d,m''} & 0 & 0 & (\mathbf{N}_k^{d,m'} \mathbf{a}) \cdot E & (\mathbf{N}_k^{d,m''} \mathbf{a}) \cdot E \end{pmatrix}.$$

Again, this simple representation holds just in case of two patches with appropriate orientations of the curves and normals. As mentioned above, the combinatorics will in general not allow such closed representations.

Analogous to the developability condition, we normalize the rows in order to prevent outliers by multiplication with a constant factor, in this case $\frac{1}{|a'(u_k)|}$ resp. $\frac{1}{|a''(u_k)|}$.

5.2.5 Isometry constraints

The developability and curve crease constraint ensure local developability in surfaces joined along common curves¹. Since we want to mimic curved crease origami, we want to specify the development as an additional constraint.

Given a polynomial developable surface, the developed surface is in general not polynomial. Therefore this condition is again just an approximation. Nevertheless, as in the case of the curved crease constraint, we are able to achieve sufficient accuracy with an approach which is based on ideas in [11]: Sampling the boundary curves of a developable surface patch appropriately yields a quad-dominant mesh with almost planar faces. The mesh obtained by successively “unrolling” the faces in the plane therefore approximates the development.

In order to avoid computing the development in every iteration, we add the vertices of the unrolled sampled mesh as two-dimensional variables \bar{v} and preserve the development through the additional *isometry constraint*

$$\sum_{(i,j)} (\|v_i - v_j\|^2 - \|\bar{v}_i - \bar{v}_j\|^2)^2,$$

where v_i, v_j are the evaluated points of the spatial curves and \bar{v}_i, \bar{v}_j the corresponding vertices in the plane, paired such that \bar{v}_i and \bar{v}_j are either neighbours or diagonals of a face of the sampled mesh.

We furthermore want to restrict the movement of the developed mesh vertices to a set of prescribed planar curves \bar{c} . Hence we add a (planar) tangent distance minimization constraint for *curve closeness*

$$\sum ((\bar{v}_i - \bar{f}_i) \cdot \bar{n}_i)^2,$$

where the \bar{f}_i denote the footpoints of \bar{v}_i on \bar{c} and \bar{n}_i the normals of \bar{c} in those points. The footpoints and normals are updated in every iteration.

We furthermore keep the corners of the sampled mesh fixed, i.e. we do not add them as variables. In order to prevent overfoldings, we apply the fairness energy term described in the following section.

Implementation

Let P_2 denote the set of parameter values of a curve obtained by equidistant sampling of the sub-parameter intervals by a (user-defined) number, that specifies the density of the sampling for the development. Since we

¹Tang et al. introduce an additional developability term for vertices. We do not support this (yet)

will evaluate the curves at these parameters in every iteration, we also compute the basis functions for the parameters P_2 in the initialization process, enabling faster evaluation later on.

Let us now schematically consider, disregarding fixed and multiple vertices, the constraint for four different lengths of a sampled face

$$F_{isom}^{face}(\mathbf{x}) = \begin{pmatrix} \|\mathbf{N}_i^{d,m} \mathbf{a} - \mathbf{N}_i^{d,m} \mathbf{b}\|^2 - \|\bar{\mathbf{a}}_i - \bar{\mathbf{b}}_i\|^2 \\ \|\mathbf{N}_{i+1}^{d,m} \mathbf{a} - \mathbf{N}_i^{d,m} \mathbf{a}\|^2 - \|\bar{\mathbf{a}}_{i+1} - \bar{\mathbf{a}}_i\|^2 \\ \|\mathbf{N}_{i+1}^{d,m} \mathbf{a} - \mathbf{N}_i^{d,m} \mathbf{b}\|^2 - \|\bar{\mathbf{a}}_{i+1} - \bar{\mathbf{b}}_i\|^2 \\ \|\mathbf{N}_i^{d,m} \mathbf{a} - \mathbf{N}_{i+1}^{d,m} \mathbf{b}\|^2 - \|\bar{\mathbf{a}}_i - \bar{\mathbf{b}}_{i+1}\|^2 \end{pmatrix} \quad \text{with } u_i, u_{i+1} \in P_2$$

for the simplified variables vector $\mathbf{x} = (\mathbf{a}, \mathbf{b}, \bar{\mathbf{a}}_i, \bar{\mathbf{a}}_{i+1}, \bar{\mathbf{b}}_i, \bar{\mathbf{b}}_{i+1})^t$. Thus the gradient $\nabla F_{isom}^{face} = 2(F_1, F_2)$ consists of

$$F_1 = \begin{pmatrix} (\mathbf{N}_i^{d,m} \mathbf{a} - \mathbf{N}_i^{d,m} \mathbf{b}) \mathbf{N}_i^{d,m} & -(\mathbf{N}_i^{d,m} \mathbf{a} - \mathbf{N}_i^{d,m} \mathbf{b}) \mathbf{N}_i^{d,m} \\ (\mathbf{N}_{i+1}^{d,m} \mathbf{a} - \mathbf{N}_i^{d,m} \mathbf{a}) \mathbf{N}_{i+1}^{d,m} & -(\mathbf{N}_{i+1}^{d,m} \mathbf{a} - \mathbf{N}_i^{d,m} \mathbf{a}) \mathbf{N}_i^{d,m} \\ (\mathbf{N}_{i+1}^{d,m} \mathbf{a} - \mathbf{N}_i^{d,m} \mathbf{b}) \mathbf{N}_{i+1}^{d,m} & -(\mathbf{N}_{i+1}^{d,m} \mathbf{a} - \mathbf{N}_i^{d,m} \mathbf{b}) \mathbf{N}_i^{d,m} \\ (\mathbf{N}_i^{d,m} \mathbf{a} - \mathbf{N}_{i+1}^{d,m} \mathbf{b}) \mathbf{N}_i^{d,m} & -(\mathbf{N}_i^{d,m} \mathbf{a} - \mathbf{N}_{i+1}^{d,m} \mathbf{b}) \mathbf{N}_{i+1}^{d,m} \end{pmatrix}$$

and

$$F_2 = \begin{pmatrix} -(\bar{\mathbf{a}}_i - \bar{\mathbf{b}}_i)^t & & (\bar{\mathbf{a}}_i - \bar{\mathbf{b}}_i)^t & \\ (\bar{\mathbf{a}}_{i+1} - \bar{\mathbf{a}}_i)^t & -(\bar{\mathbf{a}}_{i+1} - \bar{\mathbf{a}}_i)^t & & \\ -(\bar{\mathbf{a}}_i - \bar{\mathbf{b}}_{i+1})^t & -(\bar{\mathbf{a}}_{i+1} - \bar{\mathbf{b}}_i)^t & (\bar{\mathbf{a}}_{i+1} - \bar{\mathbf{b}}_i)^t & \\ & & & (\bar{\mathbf{a}}_i - \bar{\mathbf{b}}_{i+1})^t \end{pmatrix}.$$

Secondly, given a vertex $\bar{\mathbf{v}}_i$, the linear tangent distance minimization, short TDM, reads

$$F_{TDM}(\bar{\mathbf{v}}_i) = (\bar{\mathbf{v}}_i - \bar{f}_i) \bar{n}_i,$$

and thus the gradient is simply

$$\nabla F_{TDM}(\bar{\mathbf{v}}_i) = \bar{n}_i^t.$$

These isometry-facilitating constraints also act as additional regularization: when looking at the first equation of the developability condition, the optimization could work towards minimizing the distance of the curves. These constraints will in general antagonize that effect.

5.2.6 Fairness energy constraint

It may seem unnecessary to use additional fairness constraints for B-splines, but nevertheless a supplementary smoothing of the control point structure

yields more appealing surfaces in practice. We therefore minimize the following *fairness energy*

$$\sum_{i=1}^{m-1} \|a_{i-1} - 2a_i + a_{i+1}\|^2 \quad (5.4)$$

for the control points a_i with $i = 0, \dots, m$ of every curve.

We also use this constraint in a (two-dimensional) analogous way for the sampled polylines of the developed mesh.

Implementation

Assuming all vertices to be different and variable for compact notation, the corresponding linear function reads

$$F_{fair}(\mathbf{a}) = \begin{pmatrix} a_0 - 2a_1 + a_2 \\ \vdots \\ a_{m-2} - 2a_{m-1} + a_m \end{pmatrix} = \mathbf{F} \mathbf{a}$$

with

$$\mathbf{F} = \begin{pmatrix} I_3 & -2I_3 & I_3 & & & & \\ & I_3 & -2I_3 & I_3 & & & \\ & & & \vdots & & & \\ & & & I_3 & -2I_3 & I_3 & \\ & & & & I_3 & -2I_3 & I_3 \end{pmatrix}.$$

Obviously,

$$\nabla F_{fair} = \mathbf{F}.$$

Since \mathbf{F} is constant, it can be precomputed during the initialization.

Remark: Also in case of fixed or multiple control points, the fairness energy can be expressed in a sum of linear squares of the entries of $F_{fair} = \mathbf{F} \mathbf{a} + \mathbf{b}$, with a constant vector \mathbf{b} .

5.2.7 Regularization constraint

In order to prevent big variations from the input, we use the additional *Tychonoff constraint*

$$\|x - x_k\|^2, \quad (5.5)$$

where x_k stands for the last iterate.

Implementation

Denoting the identity matrix by I , the corresponding linear function for the vector of variables \mathbf{x} reads

$$F_{reg}(\mathbf{x}) = \mathbf{x} - x_k,$$

and thus

$$\nabla F_{reg} = I.$$

5.3 Combinatorial consistency

As mentioned in the introduction, the combinatorial information of the composite developables is stored in a mesh, where every face corresponds to one of the five types of surface patches, and the edges correspond to the boundary curves, labeled accordingly with either s , r or p .

In our approach, this underlying mesh serves just for combinatorial purposes, i.e. the positions of the vertices do not matter. For efficient data management between the mesh structure and optimization algorithm, the (current) geometric information is stored in external arrays, which are linked to the mesh via vertex, (half-)edge and face properties. We will skip a detailed description of the implementation here. Nevertheless, it should be pointed out that because of the assumptions made in the previous section, the underlying data must be consistent in the following ways:

- *face*: A face has at least four boundary edges. If a face has four boundary edges, at most 2 of them are labeled with s . In case of higher valence, the adjacent edges must be rulings.
- *edge-face*: If a face is bounded by two splines, the number of control points and the degree must be the same. Furthermore, we assume them to be parametrized over the same knot sequence.
- *edge-edge*: The splines/rulings meeting in a vertex must have the same first resp. last control point, since just one variable will be initialized for them.

Since we use the second consistency assumption only to count the number of needed evaluation parameters, we can generalize our constraints for surfaces with different numbers of control points and degree by choosing P_1 accordingly.

5.4 Accompanying program

The “core program” using the optimization discussed above consists of five phases:

- *Phase 1:* We start by defining the combinatorics of the underlying mesh.
- *Phase 2:* We prescribe the development, i.e. curves, whose control points will be dragged. By the end of this phase, we can prepare the B-spline basis functions of the curves for P_1 .
- *Phase 3:* Now, further properties can be set, e.g. the development settings, weights, usage of normal spline, solver settings,... Finalizing this phase enables computation of basis functions, i.e. normal spline and for P_2 , if necessary. We also set up the optimization problem, since the dimensions of the variables are known at this point.
- *Phase 4:* We define the spatial curves (by movement of vertices). Ending this phase runs the optimization.
- *Phase 5:* The optimized results can be retrieved.

This process is implemented in the interface of the plug-in RRDevelopable in the following way:

- Firstly, the user prescribes the developed curves, implicitly finalizing phase 2.
- After that, further properties can be set. By choosing a curve for control point dragging, the user finalizes phase 3.
- By selecting a control point, the user defines the updated variables. By dragging this control point, phase 4 is called with a low number of iterations to give immediate visual feedback in every mouse position with phase 5. By releasing the mouse, phase 4 is called with a higher number of iterations and the final optimizations results are retrieved with phase 5.
- Unless the user exits the plug-in, we return to the start of phase 4.

5.5 Further implementation features

Additionally, we would like to mention further implementation details, that eventually yield better results:

- *Data preprocessing:* In order to prevent loss of significance in our computations, we move the input data to the origin and scale it before running the computations. The output is transformed back again.
- *Scaling of weights:* To make the weights comparable between different examples, we scale them accordingly, i.e. we take the sampling factors into account in the case of the normal spline and development.
- *Softening of the constraints at the boundaries:* The edges labeled as rulings remain rulings throughout the optimization process. Since this is in some cases a huge restriction when it comes to the freedom of movement of the neighbouring rulings, we either suggest inscribing the face into a lense, i.e. a face with labels *spsp*, or we provide the possibility to additionally lower the weights of the developability and crease conditions by multiplication with a piecewise linear function w with user-defined breaking points $0 \leq \xi_1 \leq \xi_2 \leq \xi_3 \leq \xi_4 \leq 1$, see fig. 5.1. This usually yields better results in the middle parts of the surface patches. An obvious drawback is the additional trimming of the surfaces.

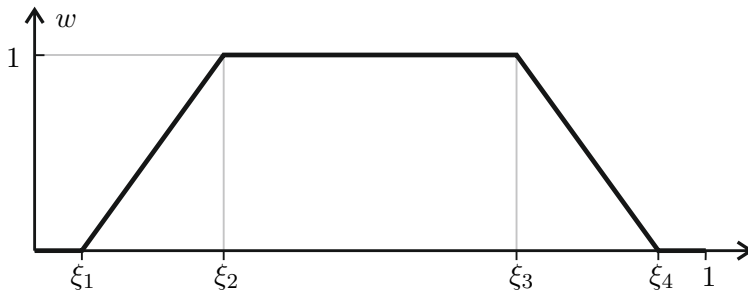


Figure 5.1: multiplicative weight function for the developability and curved crease condition

5.6 Parameters

This setup offers many possibilities to adjust the optimization to a given problem since there are many parameters one can choose from. An overview of the constraints and corresponding parameters is given in the following table:

	control points	normal		sampled mesh
		vectors	spline	
F_{dev}	1	1	$1^{(s_1)}$	
F_{fold}	1	1	$1^{(s_1)}$	
F_{unit}		ε_3	$\varepsilon_3^{(s_1)}$	
F_{isom}				$1^{(s_2)}$
F_{TDM}				$1^{(s_2)}$
F_{fair}	ε_1			$\varepsilon_1^{(s_2)}$
F_{reg}	ε_2	ε_2	ε_2	ε_2

The superscript (s_i) stands for the scaling with the appropriate sampling factor, as referred to in section 5.5.

It is of course possible to differentiate further between the weights for the different types of variables. Moreover, we collected the following parameters:

- *reduction factor for ε_2* : We decrease the weight of the fairness constraints by multiplication by a factor f_{ε_1} with $f_{\varepsilon_1} < 1$, i.e. the actual weight in the i -th iteration reads $\varepsilon_1 f_{\varepsilon_1}^i$.
- *number of intermediate and final iterations*: The proximity of the initial values to a plausible result has an impact on the number of iterations needed to achieve a good approximation. As the changes in the control points are not huge in the interactive design approach, we usually do 20 iterations per intermediate and 100 iterations in the final mouse position. However, for larger mouse moves like in the following examples, more intermediate iterations are necessary since the “errors” from the previous results seem to accumulate.
- *sampling of the developed mesh*: Experiments yield, that a sampling factor of 3 is in some cases already sufficient and the results do not differ much from those obtained from tests with a higher sampling, see fig. 5.2.
- *normal spline settings*: The user can also define the number of control points and the degree of the approximating normal spline. We still need to do some tests to see how this impacts the resulting shapes.
- *parameters of the piecewise linear function for softening weights*: The user can define the breaking points of the piecewise linear function for softening of the weights at boundaries.
- *regularization weight for moving points*: By the value of the weight for the regularization of the moving point, it is possible to express the

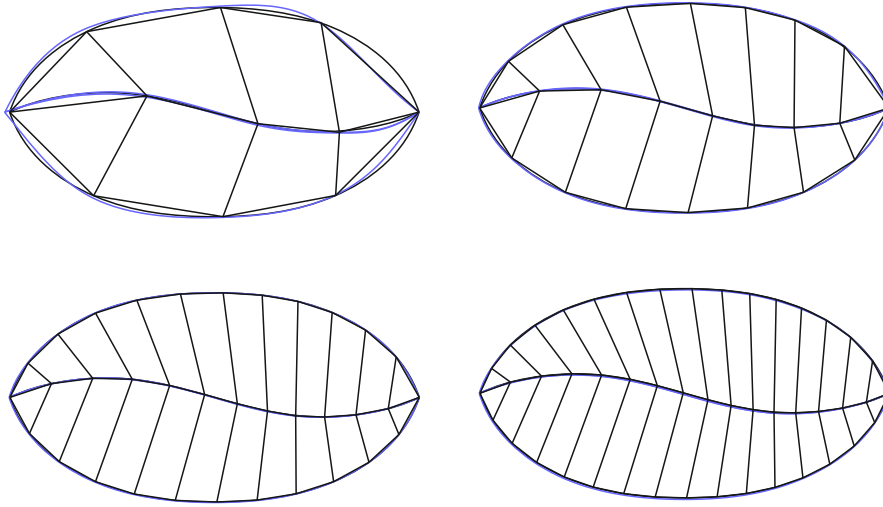


Figure 5.2: Developed boundary curves of the optimized surfaces (blue) and sampled meshes (black) for the sampling factors 1, 2, 3 and 4. The settings are those of the example below, the developed surfaces correspond to the final position.

importance of the positions of the moving points. We usually assign $100\varepsilon_2$.

In the following example, we would like to illustrate the robustness of the solver w.r.t. the choice of parameters ε_1 , ε_2 and ε_3 .

5.6.1 Robustness

The underlying geometry consists of two surface patches meeting at a common boundary curve with an inflection point. The cubic curves have seven control points. We will move one control point via three intermediate positions to its final position.

General settings

The secondary parameters mentioned above are in this case the following: We choose $f_{\varepsilon_1} = 0.8$. As the mouse movements are rather big, we choose the number of intermediate iterations to be 50. In the final position we compute 100 iterations. The sampling factor of the developed mesh is 3. Although we scale the weights accordingly, we find that the quality of our results achieved for fixed parameters ε_i varies with the sampling factor for the developed mesh. In order to reduce further parameters, we

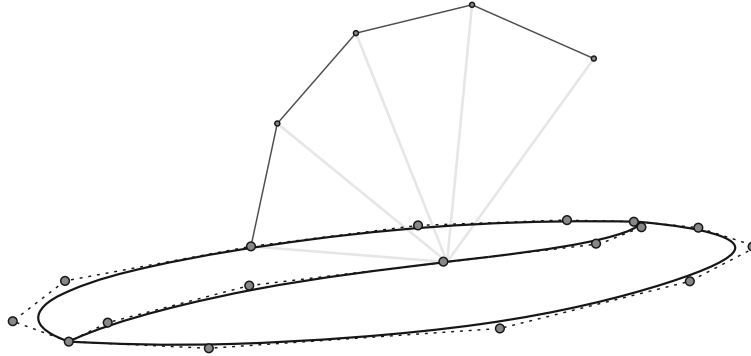


Figure 5.3: input curves and mouse positions

choose to represent our normals through normal vectors in this example. We also utilize the relaxation of the weights at the boundary with break-points $(b_0, b_1, b_2, b_3) = (0, 0.05, 0.95, 1)$ of the linear function. Finally, the Tychonoff regularization weight of the moving control point is chosen to be $100\varepsilon_2$.

Statistics

This problem has therefore in total 285 variables, i.e. the input dimension, and 822 constraints, i.e. the output dimension.

Those are partitioned as follows:

variable type	dim
control points	51
normal vectors	168
sampled mesh (2D)	66

constraint type	dim
Tychonoff	285
fairness	111
developability	168
fold	56
isometry	110
TDM	33
moving point	3

Results

We run the optimization for weights of the fairness energy $\varepsilon_1 = 10^{-k}$, the Tychonoff regularization $\varepsilon_2 = 10^{-l}0.8^i$ and unit length $\varepsilon_3 = 10^{-m}$ for $(k, l, m) \in \{4, \dots, 7\} \times \{0, \dots, 7\} \times \{0, \dots, 7\}$. The resulting final surfaces are displayed in fig. 5.4 in a grid. The values of the corresponding weights decrease along the coordinate axes.

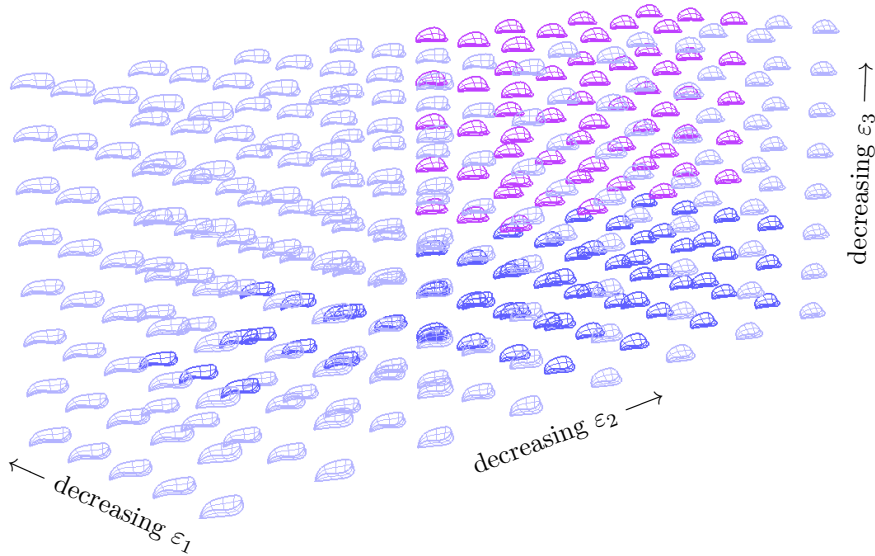


Figure 5.4: results for different combinations of the weights $(\varepsilon_1, \varepsilon_2, \varepsilon_3)$

The color-encoding should represent the following rough analysis of the surfaces:

- *pink*: Encodes surfaces with “higher” Gaussian curvature, and therefore those who are “less” developable. This may be the result of vanishing normals, due to a low weight for unit length.
- *light purple*: Encodes surfaces with a “high” residual of the isometry constraint, i.e. whose developments do not match the starting curves so well. This may be the result of an insufficient number of iterations or unsuitable combination of weights.
- *blue*: These are the surfaces that have sufficiently low residual values.

In conclusion, we obtain overall good results for $(k, l, m) \in \{5, 6, 7, 8\} \times \{1, \dots, 8\} \times \{1, 2\}$ for the above stated general settings.

5.6.2 Detailed discussion of a good result

In the following, we examine the resulting surfaces of the optimization process for the weights $(\varepsilon_1, \varepsilon_2, \varepsilon_3) = (10^{-5}, 10^{-2}, 10^{-2})$. The intermediate and final surfaces and their developments are displayed in fig. 5.5 and fig. 5.6.

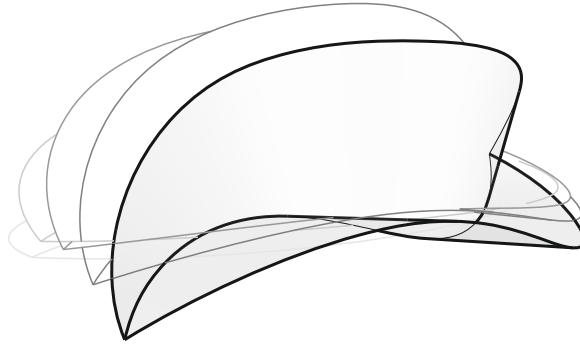


Figure 5.5: evolution of the optimized surfaces for the weights $(\varepsilon_1, \varepsilon_2, \varepsilon_3) = (10^{-5}, 10^{-2}, 10^{-2})$.

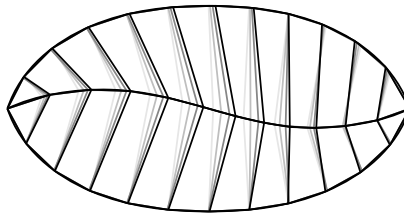


Figure 5.6: optimized sampled meshes of the surfaces in fig. 5.5 (left) and the development of the surfaces after the final optimization (right).

Residuals

We illustrate the behaviour of the weighted L^2 -residuals $\varepsilon_{cond} \|F_{cond}\|^2$ of the iterations in the optimization problem for the first and last mouse move in fig. 5.7 and 5.8 and observe the following:

Since we initialize the normals in every mouse move, we have a zero unit length residual in both first iterations. The sampled mesh also has a zero curve closeness residual in the first iteration of the first mouse move, but as the optimized sampled mesh is used for the initialization in the mouse moves to follow, the residual in general will not be 0.

As we approximate with splines and demand slightly incompatible constraints, we only get an approximation of a developable with a crease. Thus, we witness a huge drop of the residuals in the first iterations and little changes afterwards.

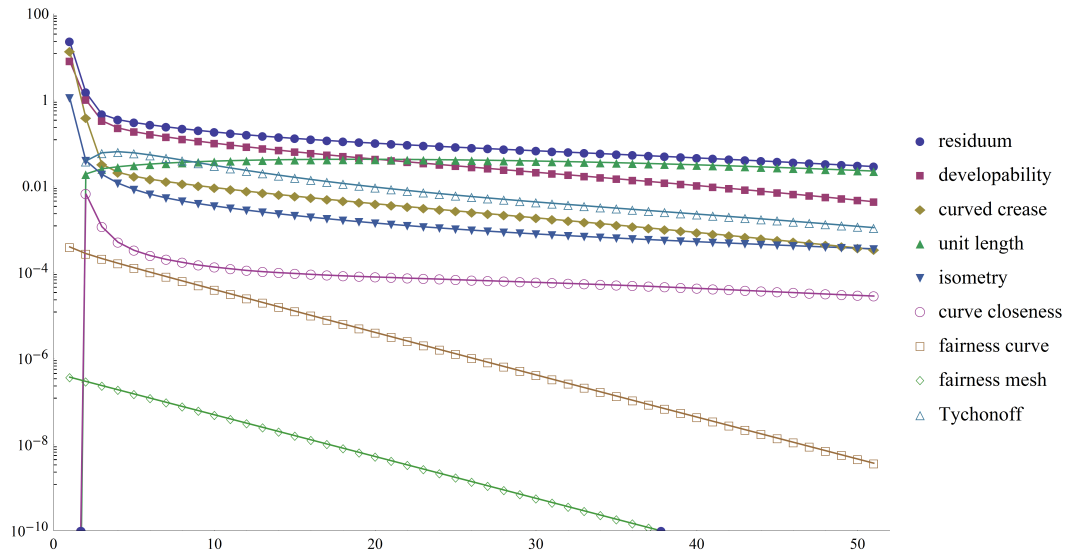


Figure 5.7: weighted residuals of the iterations after the first mouse move

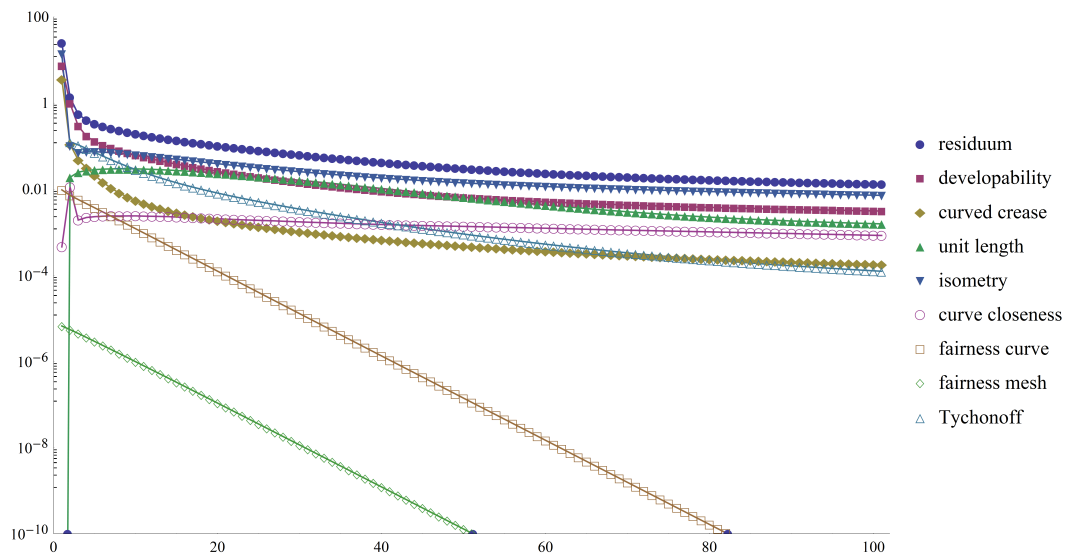


Figure 5.8: weighted residuals of the iterations after the last mouse move

Computation times

The following times (in sec.) for the evaluation of curves during the optimization process, preparation of the normal equations and solving of the resulting linear system of equations refer to a intel-core i5-4210u processor.

	number of iterations	evaluation	normal equations	solve
position 1	50	0.447	0.063	0.06
position 2	50	0.744	0.54	0.67
position 3	50	0.821	0.047	0.069
position 4	100	2.085	0.066	0.12

5.7 Convergence

The main idea of the solver in the guided projection algorithm is to describe a given problem through at most quadratic, zero-residual hard-constraints. Since this setting would be insufficient to determine a satisfying solution, additional fairness constraints, whose weights decrease to zero as the iterations progress, are added as soft energies.

Although some of our constraints, e.g. the curved crease and the isometry related conditions, are not zero-residual and are partially incoherent because of our approximations, we nevertheless use this approach. Not surprisingly, we therefore encounter a steep decrease of the residuals in the first iterations, but little changes afterwards. The tables in fig. 5.9 and fig. 5.10 show the residuals of the iterations after the first mouse move with with 1000 resp. more than 3600 iterations. Anyway, the result obtained after the first iterations is usually sufficient for our approximations of developables with curved creases.

If we just enforce zero-residual hard-constraints, i.e. the developability condition (and thus unit length), with the Tychonoff-regularization, our algorithm terminates after one iteration since this geometric constraint is fulfilled. Nevertheless, the output will not be visually appealing very often. Fig. 5.11 shows the weighted residuals of this reduced problem after adding the fairness curve constraint. It can be observed, that the only non-zero residual corresponds to the fairness constraint.

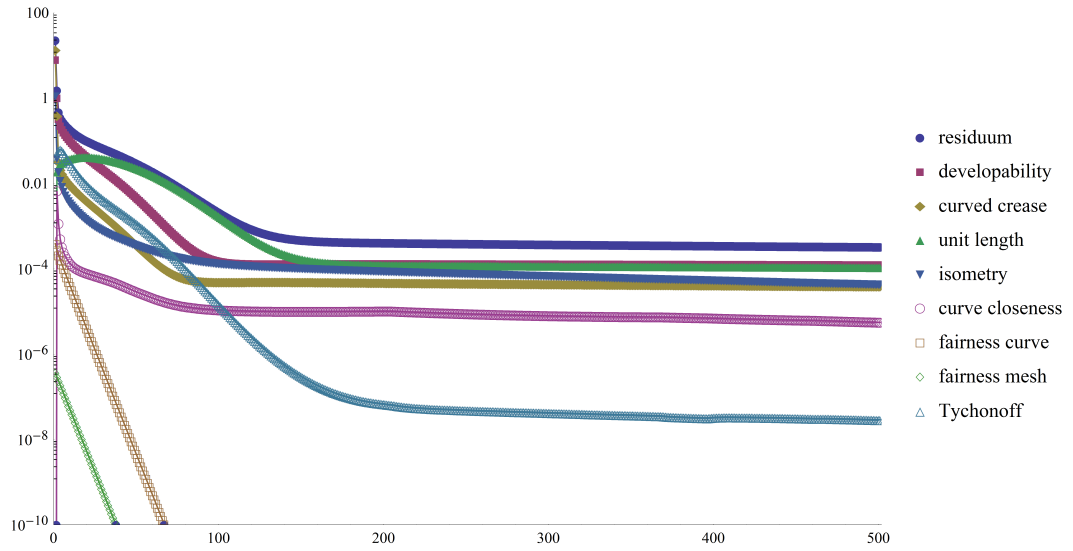


Figure 5.9: weighted residuals of the iterations after the first mouse move

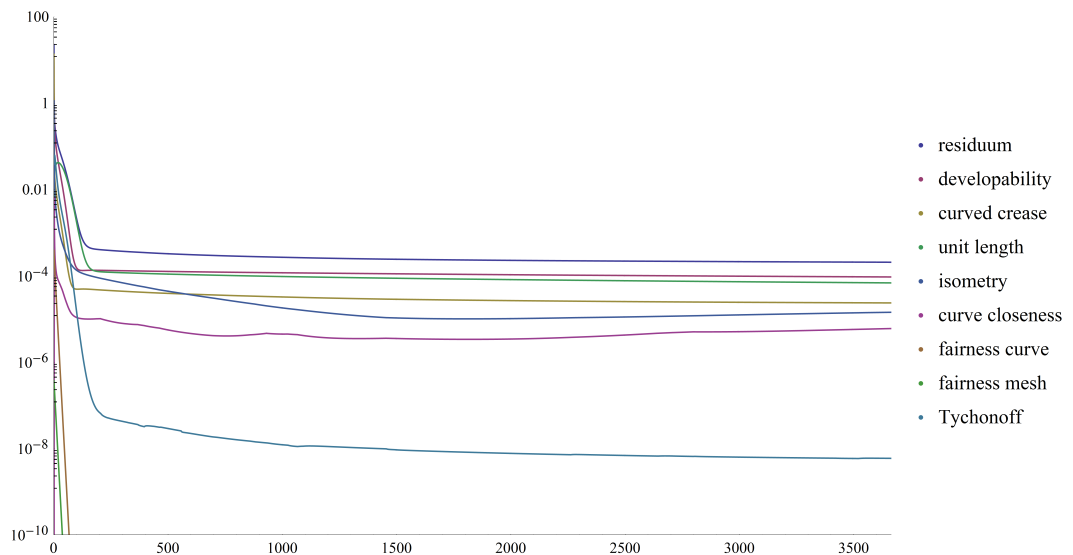


Figure 5.10: weighted residuals of the iterations after the first mouse move, stopping at a change in the objective function less than 10^{-5}

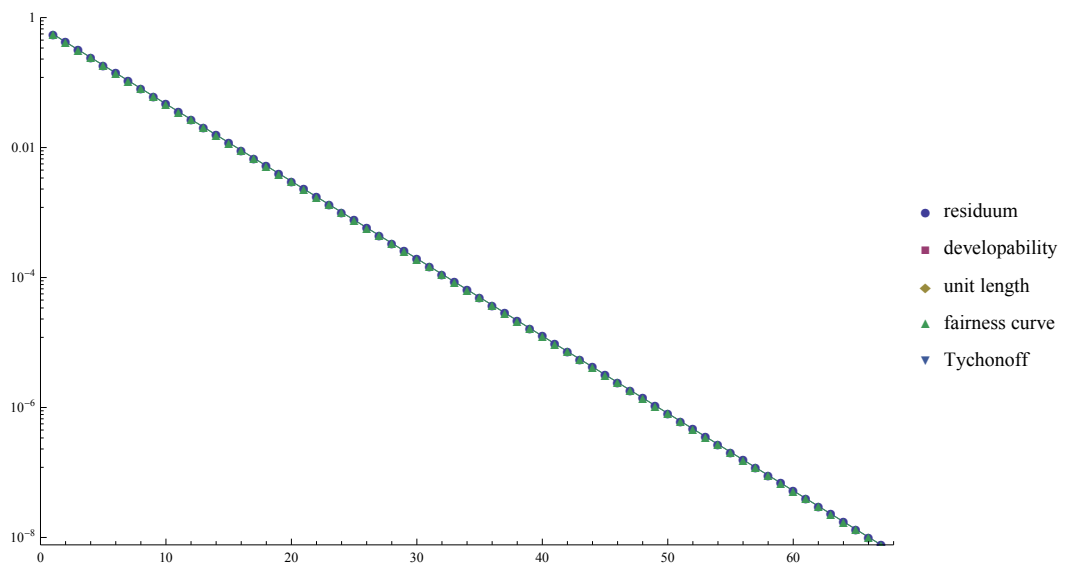


Figure 5.11: weighted residuals of a reduced problem

Chapter 6

Further examples

6.1 Moebius strip

As an example, we simulate the bending of a planar surface patch to a Moebius strip. Fig. 6.1 shows the given input curves, i.e. (straight) cubic splines with 15 control points, and the mouse positions of the first and last control points.

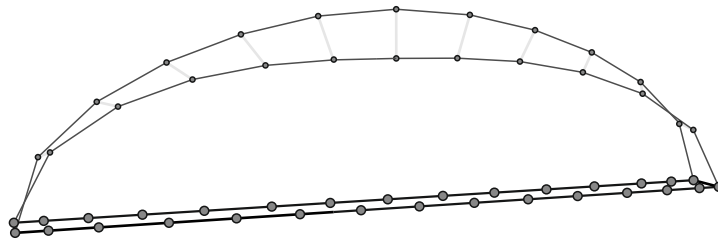


Figure 6.1: input curves and mouse positions

To facilitate continuous closure, we impose further conditions to the boundary normals and second and next to last control points in the final mouse move.

The resulting optimized surfaces, their developments and sampled meshes are displayed in fig. 6.2 and 6.3.

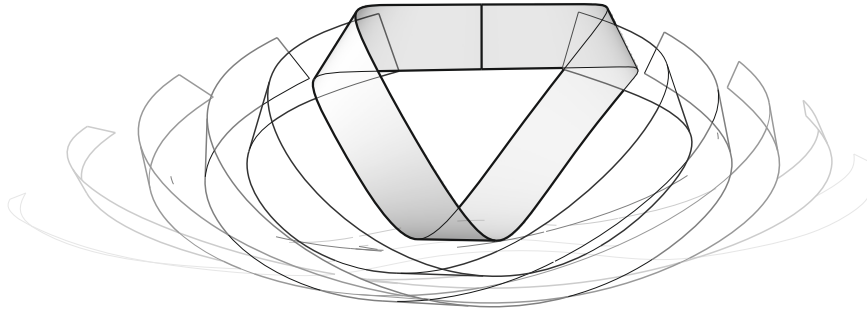


Figure 6.2: intermediate and final optimization results

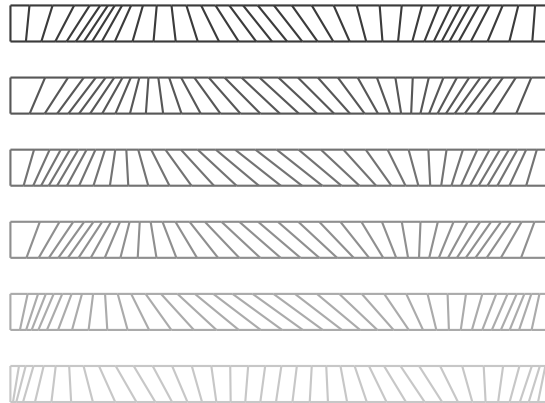


Figure 6.3: sampled meshes

6.2 Composite developable

Let us assume that we want to fold a sheet of paper along a set of prescribed creases, as in fig. 6.4.

Since the rulings will in general not be aligned to the boundaries, we extend the curves. For efficient computation, we use the combinatorics shown in fig. 6.5. Thus our mesh consists of twelve *srsp*- and three *srsr*-patches. The triangle in the middle is kept open.

We initialize a fold by moving one point downwards and applying stronger Tychonoff regularization on the three vertices of the triangle, see fig. 6.6. We also impose further constraints to the normals to preserve smooth transitions between the patches.

By moving the point downwards, we initiate a so-called “valley” crease between the two neighbouring patches. Since, given the geometry of one surface involving a curved crease defines the other surface uniquely, the type,

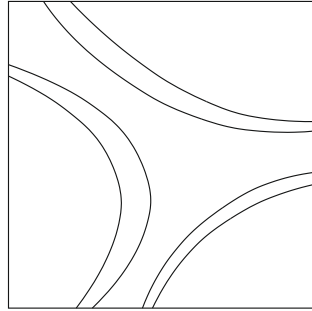


Figure 6.4: desired crease pattern

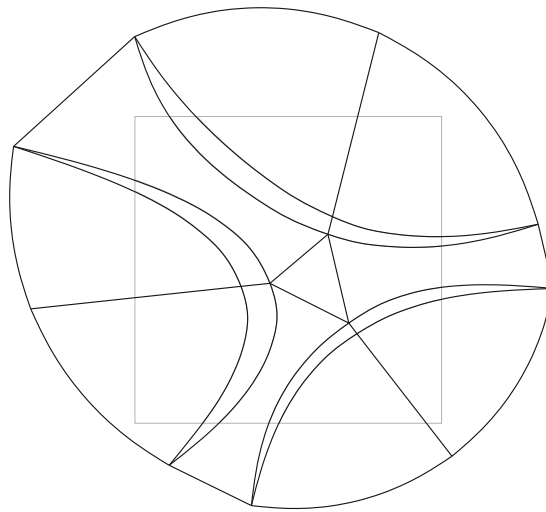


Figure 6.5: underlying combinatorics of the extended unfolding of the developable

i.e. “mountain” or “valley”, of the other creases is predetermined. We therefore do not need to and cannot prescribe the type of the crease in our approach. Nevertheless, we can achieve the desired result by initializing the movement of the control points accordingly.

For fabrication purposes, we finally trim the surfaces with a box, see fig. 6.7. Unrolling the surfaces and labeling them accordingly as mountains and valleys we obtain the fold-pattern shown in fig. 6.8, which can be used to build a model, see fig. 6.9.

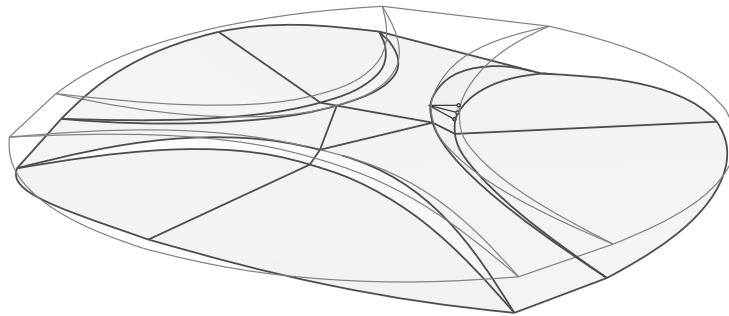


Figure 6.6: optimized surfaces for the final mouse position

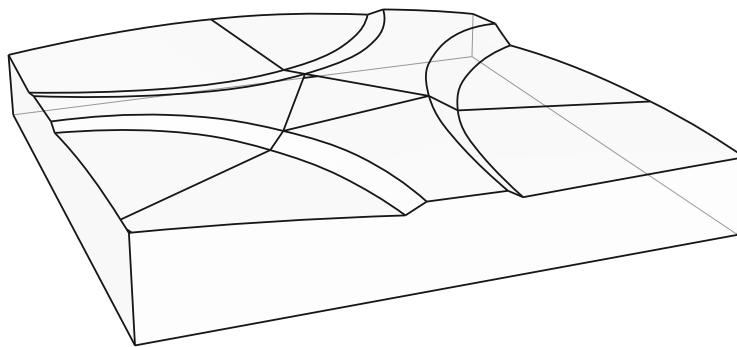


Figure 6.7: final CAD-model of the optimized surfaces

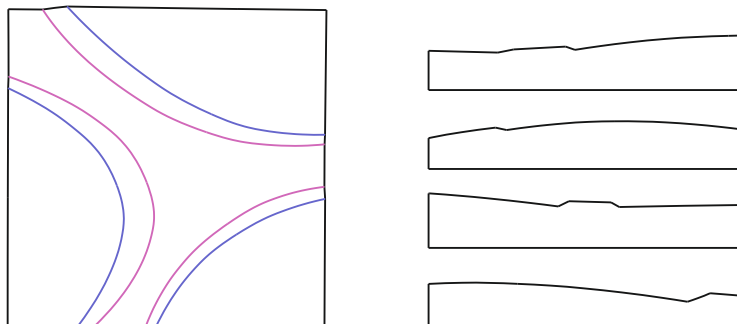


Figure 6.8: fold-pattern (the transitions between the walls of the box and the surfaces cannot be obtained by folding)



Figure 6.9: final model made out of paper and polypropylene

Bibliography

- [1] J. Boersma and J. Molenaar. *Geometry of the Shoulder of a Packaging Machine*. SIAM Review, 37, no. 3: 406–422, 1995.
- [2] E. D. Demaine, M. L. Demaine, V. Hart, G. N. Price and T. Tachi. *(Non)existence of Pleated Folds: How Paper Folds Between Creases*. CoRR, abs/0906.4747, 2009.
- [3] E. D. Demaine, M. L. Demaine, D. A. Huffman, D. Koschitz and T. Tachi. *Characterization of Curved Creases and Rulings: Design and Analysis of Lens Tessellations*. CoRR, abs/1502.03191, 2015.
- [4] E. D. Demaine, M. L. Demaine and D. Koschitz. *Reconstructing David Huffman’s Legacy in Curved-Crease Folding*. In *Origami⁵: Proceedings of the 5th International Conference on Origami in Science, Mathematics and Education (OSME 2010)*, pages 39–52. A K Peters, Singapore, 2010.
- [5] E. D. Demaine, M. L. Demaine, D. Koschitz and T. Tachi. *Curved Crease Folding: a Review on Art, Design and Mathematics*. In *Proceedings of the IABSE-IASS Symposium: Taller, Longer, Lighter (IABSE-IASS 2011)*, page to appear. London, England, 2011.
- [6] M. A. Dias, L. H. Dudte, L. Mahadevan and C. D. Santangelo. *Geometric Mechanics of Curved Crease Origami*. Phys. Rev. Lett., 109: 114301, 2012.
- [7] D. Fuchs and S. Tabachnikov. *More on Paperfolding*. Am. Math. Monthly, 106: 27–35, 1999.
- [8] D. A. Huffman. *Curvature and Creases: A Primer on Paper*. IEEE Trans. Computers, 25, no. 10: 1010–1019, 1976.
- [9] M. Kilian, S. Flöry, Z. Chen, N. J. Mitra, A. Sheffer and H. Pottmann. *Curved Folding*. ACM Transactions on Graphics, 27, no. 3: #75, 1–9, 2008.

- [10] D. Koschitz. *Computational Design with Curved Creases: David Huffman's Approach to Paperfolding*. Ph.D. thesis, MIT, 2014.
- [11] Y. Liu, H. Pottmann, J. Wallner, Y.-L. Yang and W. Wang. *Geometric Modeling with Conical Meshes and Developable Surfaces*. ACM Trans. Graph., 25, no. 3: 681–689, 2006.
- [12] G. Loria. *Spezielle algebraische und transzendente Kurven*, volume 1. Teubner-Verlag, 2nd edition, 1910.
- [13] G. Loria. *Spezielle algebraische und transzendente Kurven*, volume 2. Teubner-Verlag, 2nd edition, 1911.
- [14] J. Mitani and T. Igarashi. *Interactive Design of Planar Curved Folding by Reflection*. In *Pacific Graphics Short Papers*, edited by B.-Y. Chen, J. Kautz, T.-Y. Lee and M. C. Lin. The Eurographics Association, 2011.
- [15] H. Pottmann and J. Wallner. *Computational Line Geometry*. Springer-Verlag, 2001.
- [16] O. Röschel. *Curved Folding with Pairs of Cylinders*. In *17th International Conference on Geometry and Graphics, Beijing*. 2016.
- [17] T. Tachi and G. Epps. *Designing One-DOF Mechanisms for Architecture by Rationalizing Curved Folding*. In *Proceedings of the International Symposium on Algorithmic Design for Architecture and Urban Design*. ALGODE TOKYO, 2011.
- [18] C. Tang, P. Bo, J. Wallner and H. Pottmann. *Interactive Design of Developable Surfaces*. ACM Trans. Graph., 35, no. 2: 12:1–12:12, 2016.
- [19] W. Wunderlich. *Pseudogeodätische Linien auf Kegelflächen*. Sitzungsber., Abt. II, österr. Akad. Wiss., Math.-Naturw. Kl., 158: 75–105, 1950.
- [20] W. Wunderlich. *Pseudogeodätische Linien auf Zylinderflächen*. Sitzungsber., Abt. II, österr. Akad. Wiss., Math.-Naturw. Kl., 158: 61–73, 1950.
- [21] W. Wunderlich. *Raumkurven, die pseudogeodätische Linien eines Zylinders und eines Kegels sind*. Compos. Math., 8, 1950.
- [22] W. Wunderlich. *Raumkurven, die pseudogeodätische Linien zweier Kegel sind*. Monatsh. Math., 54: 55–70, 1950.